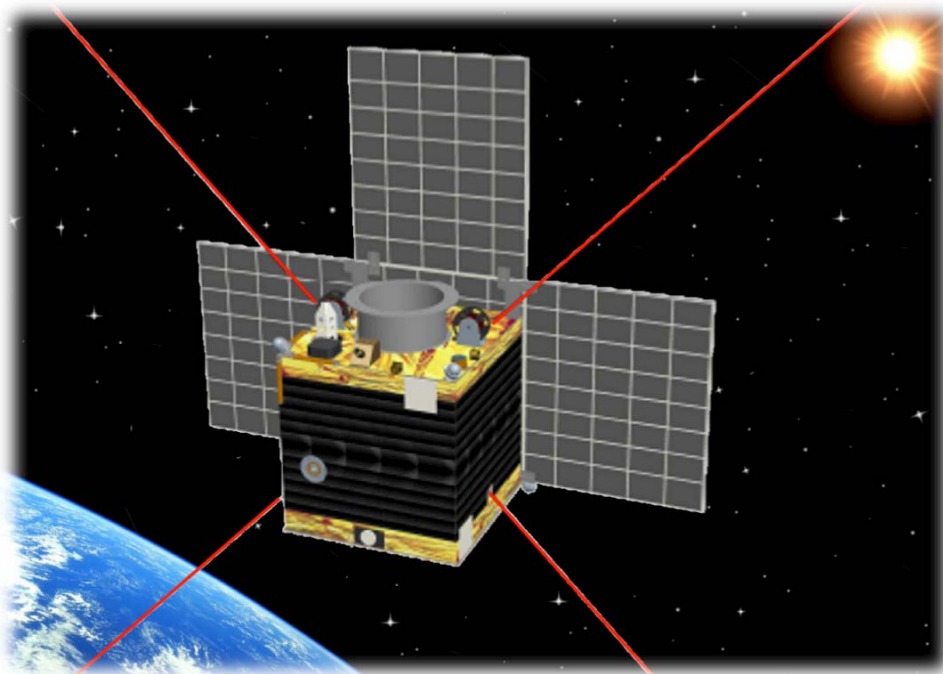


# **E-SAIL DEMO**

## **PRELIMINARY DESIGN**

### **TECHNICAL NOTE**



Prepared by <i>Preparato da</i>	A. Ruggiero, I. Andreani, P. Pergola	Date <i>Data</i>	20/11/2011
Agreed by <i>Verificato da</i>	_____	Date <i>Data</i>	20/11/2011
Approved by <i>Approvato da</i>	S. Marcuccio	Date <i>Data</i>	20/11/2011



# E-sail Demo Preliminary Design

Doc. No.: -  
Issue: 1.0  
Date: Nov. 20, 2011  
Page: 2 of 72

## DISTRIBUTION LIST

*Lista di Distribuzione*

Document Title: <i>Titolo del Documento</i>					
E-sail Demonstrator					
DISTRIBUTION <i>Distribuzione</i>	Type <i>Tipo</i>	Copies <i>Copie</i>	DISTRIBUTION <i>Distribuzione</i>	Type <i>Tipo</i>	Copies <i>Copie</i>
* Electronic Copy <i>Copia Elettronica</i>					

*This document is the property of ALTA S.p.A. - Unauthorized reproduction or distribution is not allowed.*



# E-sail Demo Preliminary Design

Doc. No.: -  
Issue: 1.0  
Date: Nov. 20, 2011  
Page: 3 of 72

## DOCUMENT CHANGE LOG

*Registrazione dei Cambiamenti*

ISSUE/ REV. <i>Versione</i>	DATE <i>Data</i>	TOTAL PAGES <i>Numero di pagine</i>	MODIFIED PAGES <i>Pagine modificate</i>	REMARKS <i>Note</i>
0.1 - DRAFT	Sept. 30, 2011			DRAFT
0.2	Oct. 20, 2011	All	All	
0.3	Oct. 28, 2011	All	All	
0.4	Nov. 11, 2011	All	All	
1.0	Nov. 20, 2011	All	All	First complete issue

---

*This document is the property of ALTA S.p.A. - Unauthorized reproduction or distribution is not allowed.*



# E-sail Demo Preliminary Design

Doc. No.: -  
Issue: 1.0  
Date: Nov. 20, 2011  
Page: 4 of 72

<b>AUTHOR (S)</b> <i>Autore/i</i>  A. Ruggiero, I. Andreani, P. Pergola	<b>ORGANIZATION (S)</b> <i>Organizzazione/i</i>  Alta S.p.a.	<b>ADDRESS</b> <i>Indirizzo</i> Alta S.p.a. Via A.Gherardesca 5, 56014 Ospedaletto (PI), Italy Phone: +39 050 985097 - Fax: +39 050 974094	
<b>TITLE</b> <i>Titolo</i>			
<b>CODE</b> <i>Codice</i>	<b>TYPE OF DOCUMENT</b> <i>Tipo di documento</i>	<b>TIME COVERED</b> <i>Tempo coperto</i>	<b>ISSUE DATE</b> <i>Data del documento</i>
<b>PROGRAMME</b> <i>Programma</i>  <input checked="" type="checkbox"/> <b>YES</b> <input type="checkbox"/> <b>NO</b>	<b>TITLE</b> <i>Titolo</i>  E-SAIL DEMO PRELIMINARY DESIGN, TECHNICAL NOTE		<b>FUNDING ORGANIZATION</b> <i>Organizzazione</i>
<b>MONITORING PERSON</b> <i>Persona di controllo</i>	<b>CONTRACT No.</b> <i>Contratto no.</i>		<b>ADDRESS</b> <i>Indirizzo</i>
<b>PROGRAMME ELEMENT</b> <i>Elemento di programma</i>	<b>TITLE</b> <i>Titolo</i>		<b>FUNDING ORGANIZATION</b> <i>Organizzazione</i>
<b>MONITORING PERSON</b> <i>Persona di controllo</i>	<b>CONTRACT No.</b> <i>Contratto no.</i>		<b>ADDRESS</b> <i>Indirizzo</i>
<b>ABSTRACT</b> <i>Estratto</i>			
<b>KEY WORDS</b> <i>Parole chiave</i>			
<b>AVAILABILITY</b> <i>Disponibilità</i>  ( ) Approved for public release; distribution is UNLIMITED ( <input checked="" type="checkbox"/> ) Approved for LIMITED distribution; no part of this document can be disclosed to third parties without written permission ( ) CLASSIFIED document only for internal use; no part of this document can be disclosed outside the company			

*This document is the property of ALTA S.p.A. - Unauthorized reproduction or distribution is not allowed.*



# E-sail Demo Preliminary Design

Doc. No.: -  
Issue: 1.0  
Date: Nov. 20, 2011  
Page: 5 of 72

## Table of Contents

### Indice

Documents.....	12
Reference Documents.....	12
1 SCOPE OF THE DOCUMENT.....	14
2 Introduction.....	15
2.1 E-sail Demonstration Mission Outline.....	15
3 Spacecraft and Mission Specifications.....	16
3.1 Launcher Interface Module.....	16
3.2 Spacecraft Configuration and Missions Phases.....	18
4 Preliminary Mission Analysis.....	22
5 Subsystem Preliminary Design.....	28
5.1 Spacecraft Propulsion Subsystem.....	34
5.2 Xenon Propellant Tank.....	36
5.3 Bang-bang Pressure Regulation Unit.....	36
5.4 Xenon Flow Control unit.....	36
5.5 Pressure Regulation Electronics.....	37
5.6 Power Supply & Control Unit.....	37
5.7 Payload.....	38
5.8 Alta Simplified FEED Thruster.....	38
5.9 Tethers and Reel Mechanism.....	39
5.10 Tether Imaging System.....	40
5.11 Colibrys SF 1500 Accelerometer.....	41
5.12 High-voltage Subsystem.....	42
5.13 Power generation Subsystem.....	43
5.13.1 PGS Preliminary Sizing.....	43
5.14 Energy Storage Subsystem.....	45
5.15 Attitude and orbit control Subsystem.....	45
5.15.1 Attitude Sensors.....	47
5.15.2 NanoSpace MEMS Cold Gas Thruster.....	49
5.15.3 Liquid Butane Propellant Tank.....	49

---

*This document is the property of ALTA S.p.A. - Unauthorized reproduction or distribution is not allowed.*



# E-sail Demo Preliminary Design

Doc. No.: -  
Issue: 1.0  
Date: Nov. 20, 2011  
Page: 6 of 72

5.15.4	Reaction Wheels Desaturation Propellant Mass Estimation .....	50
5.15.5	Magnetic Torquers.....	51
5.16	Command and Data Handling System (CDHS).....	52
5.17	Thermal control Subsystem.....	53
5.17.1	Radiator surface specification.....	54
5.18	Spacecraft Communication Subsystem.....	57
5.18.1	Antenna System.....	58
5.18.2	Antenna Switch Matrix.....	58
5.18.3	Transmitter Signal Processing Module.....	59
5.18.4	Transmitter RF Power Amplifier.....	59
5.18.5	Receiver Front-end Module.....	59
5.18.6	Receiver Signal Processing Module .....	60
5.18.7	Reference Frequency Generation Module .....	60
5.18.8	Stored Data Preliminary Estimation .....	60
5.18.9	Link Budget .....	61
5.19	Spacecraft Structure .....	65
5.19.1	Solar Panels Structure.....	66
6	Power Budget.....	67
Appendix A	.....	68

### List of figures

*Indice delle figure*

Figure 1: Artistic impression of the E-sail concept.....	15
Figure 2: Left: the ASAP-5 adapter, showing the auxiliary payload accommodation; .....	17
Figure 3: Maximum dimensions for micro auxiliary payloads. ....	18
Figure 4: Micro E-sail spacecraft configuration. In the leftmost plot the fully deployed configuration with tethers and solar panels; in the other two pictures the spacecraft in its stowed version. ....	19
Figure 5: Satellite external dimension in closed (left) and deployed solar arrays (right) configuration. ....	20
Figure 6: Schematic Representation of E-sail Demonstration Mission phases.....	21
Figure 7: Spacecraft trajectory in the geocentric inertial frame. ....	24
Figure 8: Evolution of propellant mass consumption (left) and altitude (right). ....	24
Figure 9: Evolution in time during the transfer manoeuvre of semi-major axis (top left), eccentricity (top right), Right Ascension of the Ascending Node (RAAN, bottom left) and argument of perigee (bottom right). ....	25
Figure 10: Value over mission lifetime of the incoming power (top left), spacecraft required power (top right), their difference (bottom left) and batteries state of charge (bottom right).....	26
Figure 11: External view of the spacecraft in the configuration .....	28
Figure 12: Internal view of the spacecraft.....	29
Figure 13: Internal view of the spacecraft.....	30
Figure 14: Internal view (left) and view (right) of the bottom side of the spacecraft.....	30
Figure 15: Spacecraft mass breakdown.....	31
Figure 16: Schematic representation of spacecraft with the reference frame considered for the determination of centre of mass position. ....	32
Figure 17: Alta HT-400 firing during the tests carried out in the Alta's IV4 Vacuum Chamber. ....	35
Figure 18: HT-400 Hall Effect Thruster plasma plume. ....	35
Figure 19: FEEP and Cold Gas thruster plumes with respect to spacecraft.....	39
Figure 20: Schematic representation of the tether release mechanism with .....	40
Figure 21: Schematic representation of solar panels deployment.....	43



# E-sail Demo Preliminary Design

Doc. No.: -  
Issue: 1.0  
Date: Nov. 20, 2011  
Page: 8 of 72

Figure 22: Torques generated by the Cold Gas thrusters for the desaturation of the reaction wheels. ....	46
Figure 23: Field of View of the Earth sensor (orange) and of the four Sun sensors (green). ....	48
Figure 24: Spacecraft Groundtrack. ....	62
Figure 25: Ground station visibility for the Matera ground station (left) and the Malindi ground station (right). ....	62
Figure 26: Spacecraft structure and detail of solar panels deployment joint. ....	66





# E-sail Demo Preliminary Design

Doc. No.: -  
Issue: 1.0  
Date: Nov. 20, 2011  
Page: 9 of 72

## List of tables

*Indice delle tabelle*

Table 3-1: Center of Gravity position coordinates.....	17
Table 4-1: Most relevant orbital elements of initial and target orbit.....	22
Table 4-2: Most relevant spacecraft and thruster characteristics. ....	22
Table 4-3: Natural and electric argument of perigee changing. ....	27
Table 5-1: E-sail Demo preliminary mass breakdown.....	31
Table 5-2: Centre of Gravity position coordinates for three different mission phases. ....	32
Table 5-3: Spacecraft principal Moments of Inertia. ....	32
Table 5-4: Propulsion subsystems mass breakdown. ....	34
Table 5-5: Alta's HT-400 specifications <sup>5</sup> .....	34
Table 5-6: ATK Space Systems 80326-1 Monolithic Titanium Tank specifications. ....	36
Table 5-7: Ampac Marotta UK Ltd SP05 Xenon Flow Control Unit specifications. ....	37
Table 5-8: Payload mass breakdown.....	38
Table 5-9: Alta Simplified FEED thruster specifications. ....	39
Table 5-10: Tether imaging system specifications.....	41
Table 5-11: Colibrys SF 1500 Accelerometer specifications.....	42
Table 5-12: Most relevant characteristics of AzurSpace, Emcore and .....	44
Table 5-13: Most relevant characteristic of SAFT MicroSat Li-Ion Battery Pack. ....	45
Table 5-14: AOCS mass breakdown. ....	46
Table 5-15: Astro – und Feinwerktechnik reaction RW90 wheels specifications. ....	47
Table 5-16: SSBV Fine Sun Sensor specifications .....	47
Table 5-17: SSBV Earth Horizon Sensor specifications.....	47
Table 5-18: ZARM Technik AMR digital Magnetometer specifications. ....	48
Table 5-19: NanoSpace Cold gas thruster specifications.....	49
Table 5-20: AMPAC BS25-001 stainless steel propellant tank specifications. ....	49
Table 5-21: ZARM Technik MT 1-1 Magnetic Torquers specifications.....	51
Table 5-22: CDHS characteristics.....	52
Table 5-23: Spacecraft components and relative operative and design temperature range. ....	53
Table 5-24: Main thermal radiators and layers on spacecraft <sup>20</sup> .....	54

---

*This document is the property of ALTA S.p.A. - Unauthorized reproduction or distribution is not allowed.*



# E-sail Demo Preliminary Design

Doc. No.: -  
Issue: 1.0  
Date: Nov. 20, 2011  
Page: 10 of 72

Table 5-25: Dissipated power values for the most critical components. All the others electrical components are neglected because they dissipate less than 1 W. ....	55
Table 5-26: Physical and thermo-optical properties of JDSU Optical Solar Reflectors (OSR).....	55
Table 5-27: Required heat for Xenon and Butane tanks. ....	56
Table 5-28: Spacecraft Communication Subsystem mass breakdown.....	57
Table 5-29 SSTL Micropatch antenna specifications. ....	58
Table 5-30: AntDevCo helix antenna specifications.....	58
Table 5-31: Total amount of stored data from spacecraft sensors over one orbit. ....	61
Table 5-32: Position of the candidate ground stations. ....	61
Table 5-33: Spacecraft preliminary link budget with Malindi ground station. ....	64
Table 5-34: Physical characteristics of the aluminium alloys composing the spacecraft structure. .	65
Table 5-35: Elements of spacecraft structure and their mass. ....	65
Table 6-1: Power required by the most relevant spacecraft subsystems during the mission. ....	67
Table 6-2: Power required by the spacecraft and by each subsystem .....	67

## List of acronyms and abbreviations

*Indice degli acronimi e abbreviazioni*

AOCS	Attitude and Orbit Control Subsystem
ASAP-5	Arianespace Structure for Auxiliary Payloads (Ariane 5)
ASAP-S	Arianespace Structure for Auxiliary Payloads (Soyuz)
ASI	Italian Space Agency
BCR	Battery Charge Regulator
BPRU	Bang-bang Pressure Regulation Unit
BPSK	Binary Phase Shift Keying
C&DH	Command & Data Handling
COTS	Commercial Off The Shelf
E-sail	Electric Solar Wind Sail
FEEP	Field Emission Electric Propulsion
FPGA	Field Programmable Gate Array
GAfFET	Gallium Arsenide Field Effect Transistor
GTO	Geostationary Transfer Orbit
HET	Hall Effect Thruster
HEO	High Elliptic Orbit
LDMOS	Laterally Diffused Metal Oxide Semiconductor
LNA	Low-Noise Amplifier
OBDH	On-Board Data Handling
PA	Power Amplifier
PCM	Power Conditioning Module
P-HEMT	Pseudomorphic High Electron Mobility Transistor
PGS	Power Generation Subsystem
PSCU	Power Supply & Control Unit
RF	Radio Frequency
SDR	Software Defined Radio
TCS	Thermal Control Subsystem
XFC	Xenon Flow Control
SCS	Spacecraft Communication Subsystem



# E-sail Demo Preliminary Design

Doc. No.: -  
Issue: 1.0  
Date: Nov. 20, 2011  
Page: 12 of 72

## DOCUMENTS

### Reference Documents

1. Janhunen, P., P.K. Toivanen, et al. "Electric solar wind sail: Towards test missions", Rev. Sci. Instrum., 81, 111301, 2010.
2. Ariane 5 Structure for Auxiliary Payload User's Manual, Arianespace, May 2000
3. A. Ruggiero, P. Pergola and S. Marcuccio, "Joint Trajectory and Energy Management Simulation of Low Thrust Missions," 32<sup>nd</sup> International Electric Propulsion Conference, 2011.
4. SAFT Li-ion MicroSat module datasheet  
[URL: <http://www.saftbatteries.com/doc/Documents/space/Cube712/MicroSat-8S3P.bb237a09-038a-4578-a9ae-3381ec21833a.pdf>]
5. S. Oslyak, D. Dignani, C. Ducci, P. Rossetti, M. Andrenucci, "Experimental characterization of a 400-W HET", 32nd International Electric Propulsion Conference, 2011.
6. NanoSpace MEMS Thruster Module datasheet  
[URL: <http://www.sscspace.com/file/mems-thruster-module-march.pdf>]
7. ATK Space Systems 80326-1 datasheet  
[URL: [http://www.psi-pci.com/Data\\_Sheets\\_Library/DS326.pdf](http://www.psi-pci.com/Data_Sheets_Library/DS326.pdf)]
8. Marotta UK Ltd SP05 Xenon Flow Control Unit datasheet  
[URL: [http://www.ampacispcheltenham.eu/docs/SP05\\_marotta.pdf](http://www.ampacispcheltenham.eu/docs/SP05_marotta.pdf)]
9. C. Elisabelar, J.M. Labille and J.N.Castiaux, "Low power PCDU", European Space Power Conference, Portugal 2002
10. S. Marcuccio, N. Giusti, P. Pergola, "Development of a Miniaturized Electric Propulsion System for the E-sail Project", International Astronautical Federation Congress 2011, South Africa, 2011.
11. Colibrys SF 1500 Accelerometer datasheet [URL: <http://www.colibrys.ch/e/page/184/>]
12. EMCO DX Series datasheet  
[URL: <http://www.emcohighvoltage.com/pdfs/dxseries.pdf>]
13. Astro- und Feinwerktechnik Adlershof GmbH, RW90 Reaction Wheels datasheet  
[URL: [http://www.astrofein.com/2728/dwnld/admin/Datenblatt\\_RW90.pdf](http://www.astrofein.com/2728/dwnld/admin/Datenblatt_RW90.pdf)]
14. ZARM Technik MT 1-1 Magnetic Torquers datasheet  
[URL: [http://zarm-technik.de/downloadfiles/ZARMTchnikAG\\_CubeSatTorquers\\_web2010.pdf](http://zarm-technik.de/downloadfiles/ZARMTchnikAG_CubeSatTorquers_web2010.pdf) ]
15. SSBV Space & Ground Systems UK Fine Sun Sensors datasheet  
[URL: <http://www.satserv.co.uk/New%20Sun%20Sensor.pdf>]
16. ZARM Technik AMR digital Magnetometer datasheet  
[URL: [http://zarm-technik.de/downloadfiles/ZARMTchnikAG\\_Magnetomers\\_web2010.pdf](http://zarm-technik.de/downloadfiles/ZARMTchnikAG_Magnetomers_web2010.pdf) ]
17. SSBV Earth Horizon Sensor datasheet  
[URL: <http://www.satserv.co.uk/Earth%20Horizon%20Sensor.pdf>]
18. NASA SPACE VEHICLE DESIGN CRITERIA - NASA/SP-8018 -, NASA, 1969
19. W. Ley, K. Wittmann, W. Hallmann, "Handbook of space technology," Wiley, 2009
20. J. R. Wertz, W. J. Larson, Space Mission Analysis and Design. 3rd edition, Microcosm, 1999
21. JSDU Optical Solar Reflector Datasheet, [URL: <http://www.jdsu.com>]
22. STTL Micropatch S-Band Antenna datasheet  
[URL: [http://www.sstl.co.uk/Downloads/Datasheets/S\\_Band\\_Patch\\_Antenna\\_0035528\\_v503](http://www.sstl.co.uk/Downloads/Datasheets/S_Band_Patch_Antenna_0035528_v503)]
23. AntDevCo Helix Medium Gain Antenna datasheet



# E-sail Demo Preliminary Design

Doc. No.: -  
Issue: 1.0  
Date: Nov. 20, 2011  
Page: 13 of 72

- [URL:<http://www.antdevco.com/ADC-01010841%20Helix%20Antenna%20data%20sheet.pdf>]  
24.SSTL OBC695 Radiation tolerant flight computer datasheet  
[URL:[http://www.sstl.co.uk/Downloads/Datasheets/Radiation\\_Tolerant\\_OBC695\\_0116661\\_v202](http://www.sstl.co.uk/Downloads/Datasheets/Radiation_Tolerant_OBC695_0116661_v202)]  
25.SSTL High Speed Data Recorder datasheet  
[URL: [http://www.sstl.co.uk/Downloads/Datasheets/HSDR\\_0118021\\_v116](http://www.sstl.co.uk/Downloads/Datasheets/HSDR_0118021_v116)]



# **E-sail Demo Preliminary Design**

Doc. No.: -  
Issue: 1.0  
Date: Nov. 20, 2011  
Page: 14 of 72

## **1 SCOPE OF THE DOCUMENT**

This document is a preliminary study for the E-sail Demo mission. The study was performed at Alta as an internally funded activity in the frame of the involvement of the company with the E-sail project. The experiment definition, mission profile, and various aspects of the onboard subsystems are based on work partly performed by an international team under the “E-sail” project ([www.electric-sailing.fi/fp7/](http://www.electric-sailing.fi/fp7/)), led by Pekka Janhunen of the Finnish Meteorological Institute (FMI) under FP7 funding.

Parts of the study were contributed by FMI (OBDH) and by Tartu Observatory (tether imaging system, telecommunications).

## 2 INTRODUCTION

### 2.1 E-sail Demonstration Mission Outline

The E-Sail Demo mission is a technology demonstrator for the Electric Solar Wind Sail (E-sail)<sup>1</sup>. The E-sail is an innovative, propellantless space propulsion concept based on the interaction of a number of electrically biased tethers with the protons of the solar wind (Fig. 1). An electron gun is used to keep the spacecraft and the tethers at a high positive potential with respect to the ambient plasma. The electrically effective sail area extends a few tens of meters into the surrounding solar wind plasma, so that ions composing solar wind interact with the electric field generating a net thrust acting on the spacecraft.

In the proposed technology demonstration mission of E-sail, a scaled-down version of the E-sail is used to verify generation of thrust in the real space environment. Four tethers are deployed and centrifugally stretched on the external side of a small spacecraft moving for part of its orbit outside the magnetosphere in order to intercept unperturbed solar wind. The spacecraft is injected into a Geostationary Transfer Orbit (GTO) and the orbital apogee is raised up to about 25 Earth radii by the onboard electric propulsion system. Tethers are then deployed and the electron gun is switched on to initiate E-Sail operation phase. The propulsive effect is detected both by remote tracking of the spacecraft trajectory and by onboard accelerometers.

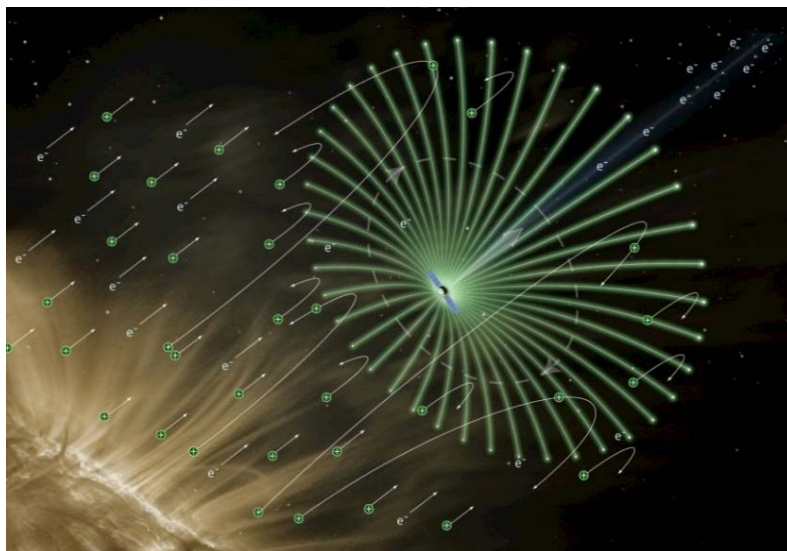


Figure 1: Artistic impression of the E-sail concept

	<b>E-sail Demo</b> <b>Preliminary Design</b>	Doc. No.: - Issue: 1.0 Date: Nov. 20, 2011 Page: 16 of 72
---	---	--

### 3 SPACECRAFT AND MISSION SPECIFICATIONS

In general the preliminary design of the the Micro E-sail Demo is conceived so as to be lightweight, compact and flexible. This would allow the possibility to board the spacecraft into a number of different small and medium class launcher either as primary payload or as piggyback. For this study, however, the baseline launch scenario assumed is a GTO direct launch as piggyback payload on board of the adapter for auxiliary payloads of the Ariane-5 launcher form Kourou.

The preliminary design of the Micro E-sail Demonstrator, thus, is based on the constraints imposed by the Arianespace Structure for Auxiliary Payload (ASAP). In particular, the spacecraft is meant to be launched as a micro auxiliary payload (mass < 120 kg) onboard the Ariane 5 ASAP (ASAP-5)<sup>2</sup>. The spacecraft mass and size are sought such that it is also compatible with the Soyuz ASAP adapter (ASAP-S). The initial spacecraft orbit is a Geosynchronous Transfer Orbit (GTO) with a perigee altitude of 600 km and an apogee altitude of 35786 km, standard specifications for Kourou GTO. The target orbit is a Highly Elliptical Orbit (HEO) with the same perigee of the initial orbit and an apogee altitude of 25 Earth radii (~ 165832 km).

Considering the high total impulse required for the orbit transfer manoeuvre, the spacecraft main propulsion system is based on a low power Hall Effect Thruster able of providing the relevant velocity increment with a small propellant mass fraction. As design drivers, we assumed a spacecraft mass upper limit of the order of 60 kg. Furthermore, to reduce cost, the use of Commercial Off The Shelf (COTS) components is preferred, possibly based on the available CubeSat technology.

#### 3.1 Launcher Interface Module

The ASAP-5 adapter (Fig. 2) is a circular platform capable of boarding up to 4 “mini” auxiliary payloads (120 kg < mass < 300 kg) or up to 8 “micro” auxiliary payloads (mass < 120 kg)<sup>2</sup>.



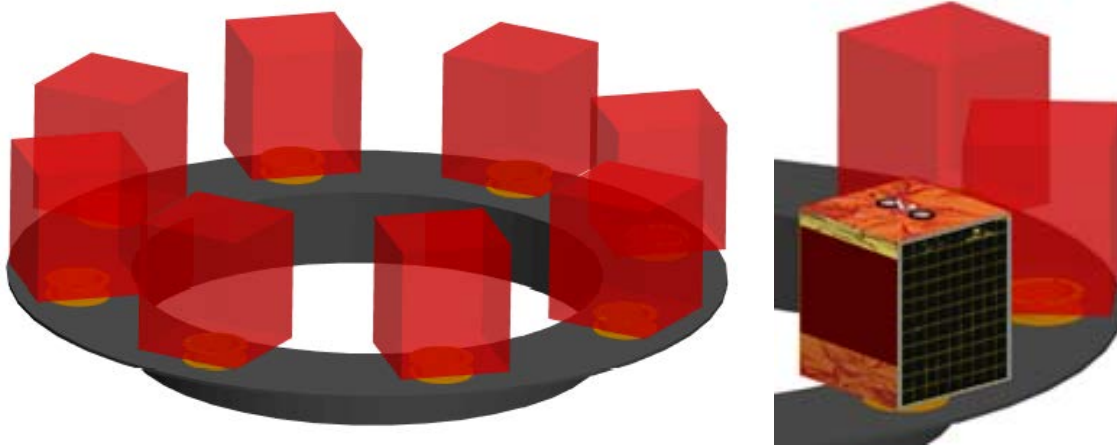


Figure 2: Left: the ASAP-5 adapter, showing the auxiliary payload accommodation; right: the E-sail demo satellite mounted on the adapter

The Micro Auxiliary Payload will be mounted on ASAP 5 with the standard separation plate provided by Arianespace. This component is already supposed to be included in the spacecraft design.

The requirements for ASAP “micro” payloads are:

- Maximum mass without separation system  $\leq 120$  kg.
- Centre of gravity position with respect to the centre of the mounting plate:

$X_G$ [mm]	$Y_G$ [mm]	$Z_G$ [mm]
$\leq \pm 5$	$\leq \pm 450$	$\leq \pm 5$

Table 3-1: Center of Gravity position coordinates

- Maximum external dimensions: 600x600x710 mm.

Figure 3 shows the maximum external size of the micro auxiliary payload lodging area.

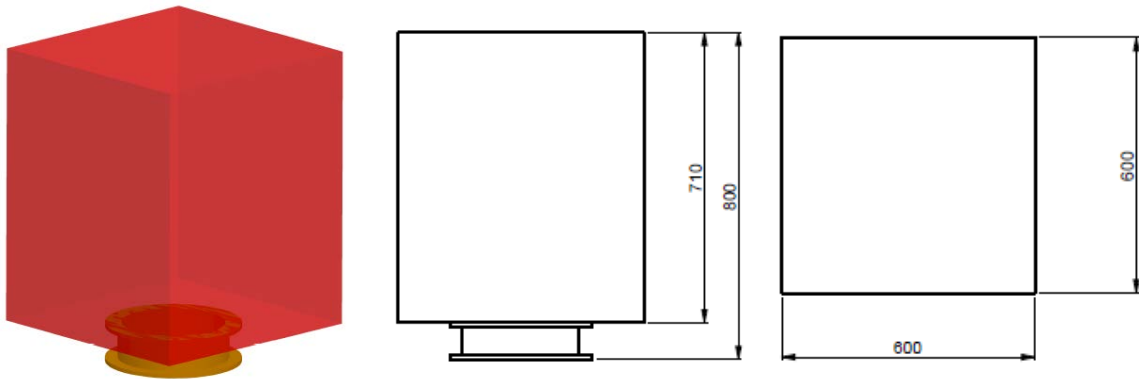


Figure 3: Maximum dimensions for micro auxiliary payloads.

### 3.2 Spacecraft Configuration and Missions Phases

External dimensions of the spacecraft are assumed to be equal to the maximum dimensions allowed by the ASAP-5 payload adapter. In order to produce the power required to operate the electric thrusters during the orbit transfer phase, the spacecraft is equipped with one body-mounted solar panel and three deployable solar arrays (Figure 4).

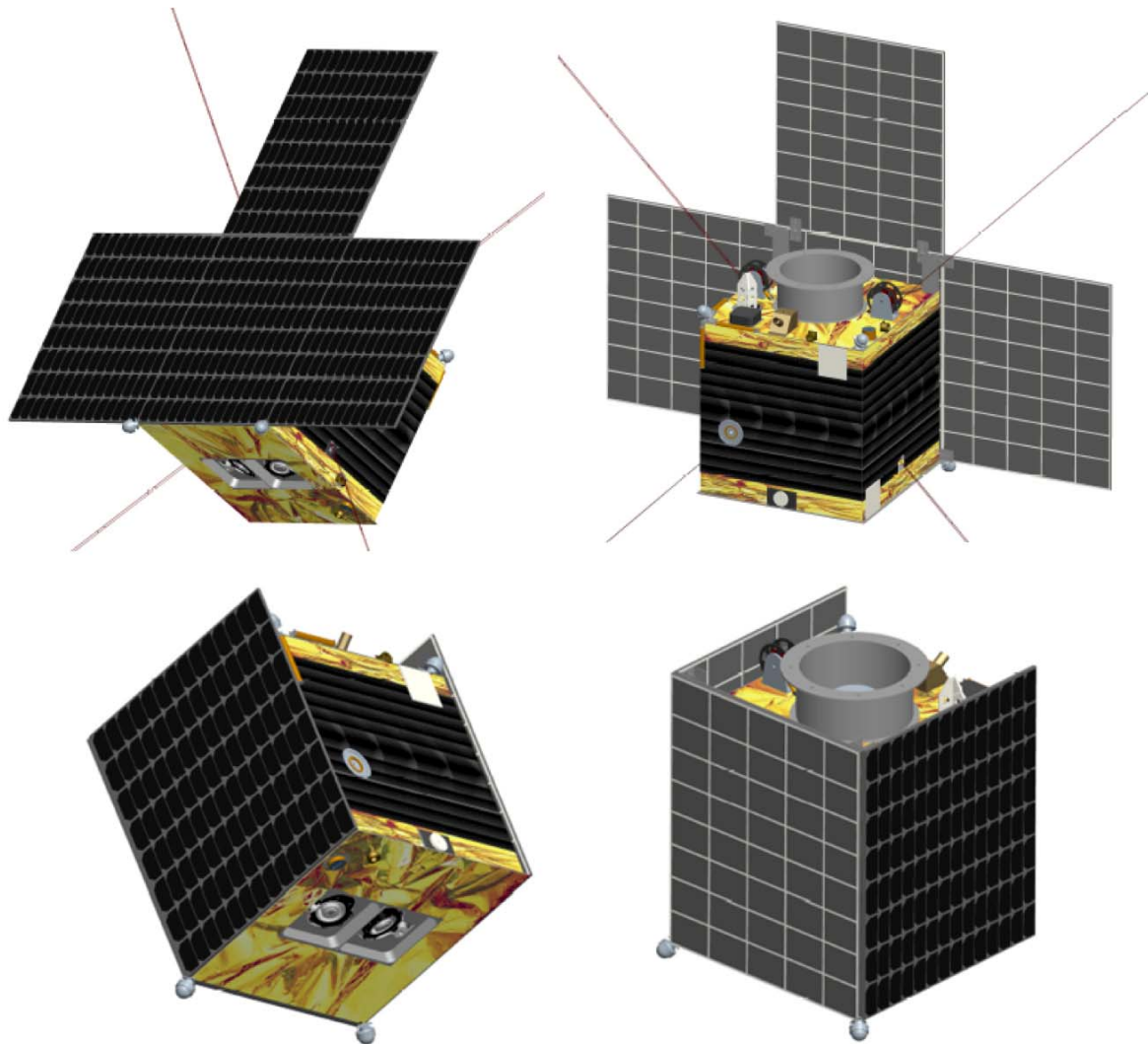


Figure 4: Micro E-sail spacecraft configuration. In the leftmost plot the fully deployed configuration with tethers and solar panels; in the other two pictures the spacecraft in its stowed version.

Figure 5 shows the satellite maximum external size both in the stowed configuration (left) and with fully deployed solar arrays (right). The stowed configuration does not exceed the maximum ASAP-5 dimensions.

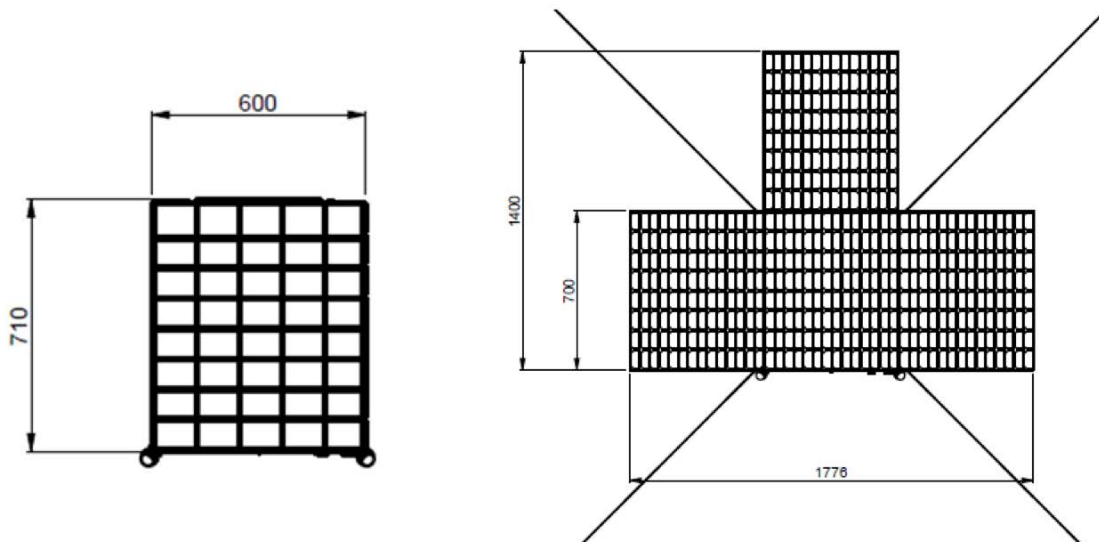


Figure 5: Satellite external dimension in closed (left) and deployed solar arrays (right) configuration.

The solution identified has the substantial advantage of providing enough power both for the spacecraft thruster and subsystems. Immediately after the spacecraft deployment, two out of six spacecraft sides are covered with solar arrays so to provide power for the telecommunication and attitude control subsystems. At the same time, spacecraft thermal control is guaranteed by the thermal control surfaces mounted on the side of the spacecraft opposite to body-mounted solar array.

This configuration is also robust in case of malfunctioning of the opening mechanism of the solar arrays. In this case, indeed, it would be still possible to perform a limited-performance mission (for instance test in space a number of innovative components).

The sequence of spacecraft manoeuvres prior to switch-on of the experiment is as follows:

1. The launcher releases the spacecraft into departure GTO.
2. LEOP, where engineers take control of the spacecraft and the status of each subsystem is monitored.
3. Telecommunication subsystem transmits spacecraft state to the ground station.
4. The attitude control subsystem starts compensating the spacecraft spin and performs Sun acquisition and then the deployable solar arrays are opened.
5. Spacecraft attitude is adapted to start the thruster operation phase.

6. Thrusters are operated following a predefined strategy (see Sec. 3):
    - a. the target orbit semi-major axis is reached by means of a series of thrusting arcs centred around orbit perigee.
    - b. afterwards the orbit eccentricity is modified up to the target value thrusting for the entire orbit along a constant direction in space (normal to orbit semi-major axis).
  7. The propulsion subsystem is switched off and the E-sail deployment is initiated.
  8. The E-sail concept demonstration phase is carried out for approximately 3 months after the end of the orbit transfer phase.
  9. At the end of payload operation phase, the spacecraft is deorbited operating again the electric propulsion system up to the complete spacecraft burning up in the Earth atmosphere.
- A schematic representation of the main mission phases is shown in Figure 6.

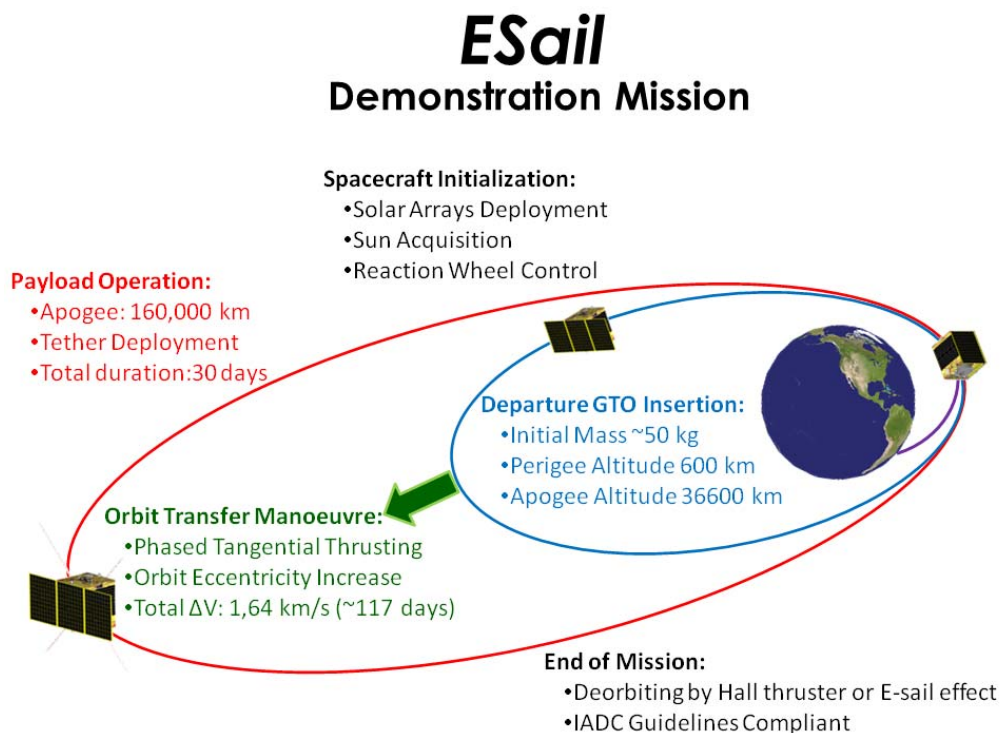


Figure 6: Schematic Representation of E-sail Demonstration Mission phases when using GTO launch.

## 4 PRELIMINARY MISSION ANALYSIS

The preliminary mission analysis of the E-sail Demo was carried out using Alta's SATSLab software package<sup>3</sup>, including an accurate low thrust orbital and attitude propagator and the onboard subsystem energy and power flux models.

Initial and target orbits parameters are listed in Table 4-1.

Orbital Element	Initial Orbit	Target Orbit
$a$	24,562,137	86,404,8495 km
$e$	0,715899	0,919239
$h_p$	600 km	600 km
$h_a$	35786 km	~159453 km

Table 4-1: Most relevant orbital elements of initial and target orbit.

The orbital perturbations taken into account during the design of the transfer manoeuvre are:

- Atmospheric drag (Harris-Priester medium density static model)
- Earth oblateness (J2-J6)
- Sun and Moon gravity fields

The mission launch date assumed is Jan. 1, 2014, and the most relevant spacecraft and thruster characteristics used for the simulations are shown in Table 4-2.

<b>Spacecraft Mass</b>	60 kg	<b>Solar Arrays Area</b>	4 x 0.426 m <sup>2</sup>
<b>Drag-exposed area</b>	1.7 m <sup>2</sup>	<b>Solar Arrays Efficiency</b>	20.5%
<b>Drag coefficient</b>	2.2	<b>Max Generated Power</b>	475 W
<b>Thrust</b>	25 mN	<b>Battery Capacity</b>	465 Wh
<b>Specific Impulse</b>	1250 s	<b>Thruster Power Consumption</b>	375 W

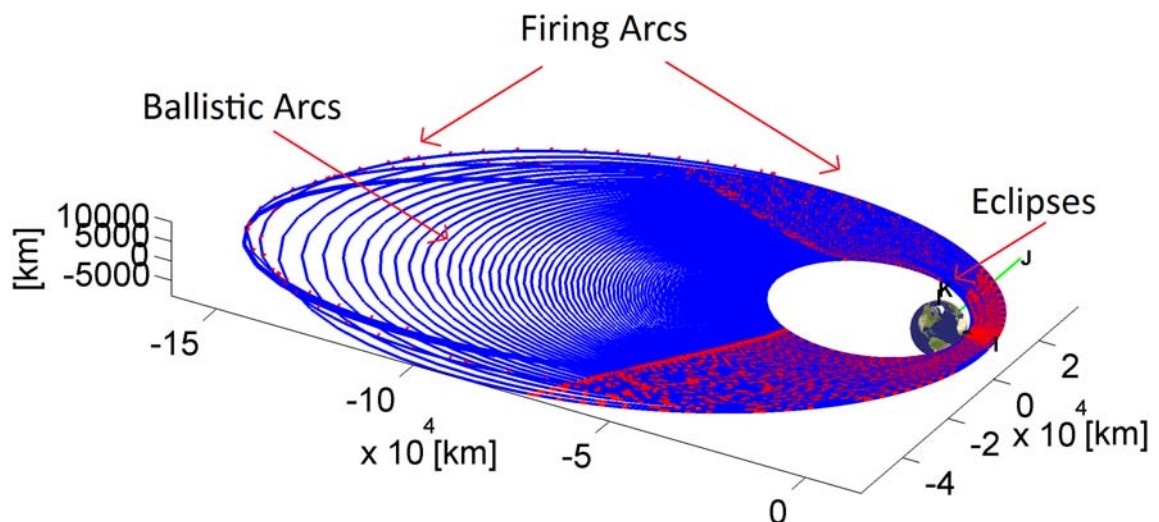
Table 4-2: Most relevant spacecraft and thruster characteristics.

The default thrusting strategy considered envisages to first increase the orbit semi-major axis by means of a series of tangential thrusting firing arcs centred around orbit perigee, then the orbit eccentricity is increased up to target value thrusting for the entire orbit along a constant direction in space (normal to orbit semi-major axis). The attitude of the spacecraft is continuously controlled by means of 4 reaction wheels mounted in tetrahedral configuration that have to be unloaded by means of cold gas thrusters and magnetorquers.

Considering the thruster power requirements, the spacecraft is assumed to be equipped with 4 solar arrays of about  $0.426 \text{ m}^2$  each mounted on one side of the structure so that the thrust vector is always perpendicular to the normal to the solar panels. Thus, the instantaneous value of the power generated by the solar panels is obtained considering the instantaneous angle between Sun-Spacecraft relative position vector and the normal to thrust direction (i.e., the normal to the solar panels). The arrays have an average overall efficiency of about 20.5% and are able to provide a maximum of 475 W of power. The low value of the overall solar arrays efficiency has been assumed to take into account of solar cells degradation and of the non-complete coverage of the solar panels with solar cells.

The energy produced by solar panels is stored in a single 465 Wh SAFT Li-ion MicroSat module4 (see Sec. 5.14). The thruster does not operate during eclipse phases and when the depth of discharge of the batteries is larger than 50%. The power required by all other subsystems has been accounted for, in a very conservative way, by introducing a constant power consumption of 55 W (Sec. 5 for the detailed power budget).

The transfer manoeuvre requires about 7.5 kg of propellant (~12.4% of the initial mass) and a transfer time of about 128 days. The total velocity increment corresponding to the performed manoeuvre is about 1.62 km/s with about 1000 hours of cumulative thruster firing time.



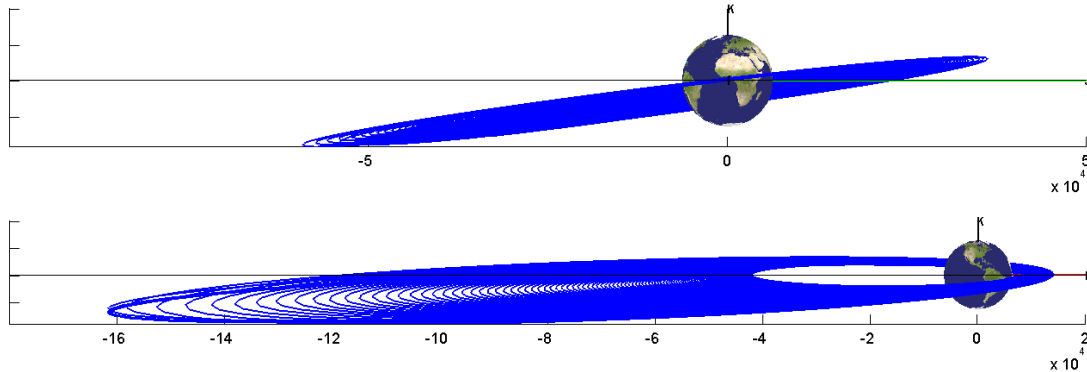


Figure 7: Spacecraft trajectory in the geocentric inertial frame.  
 Red dots indicate thrusting arcs; coasting phases are shown in blue.

Figure 8 shows the propellant mass consumption and the altitude evolution along the whole trajectory.

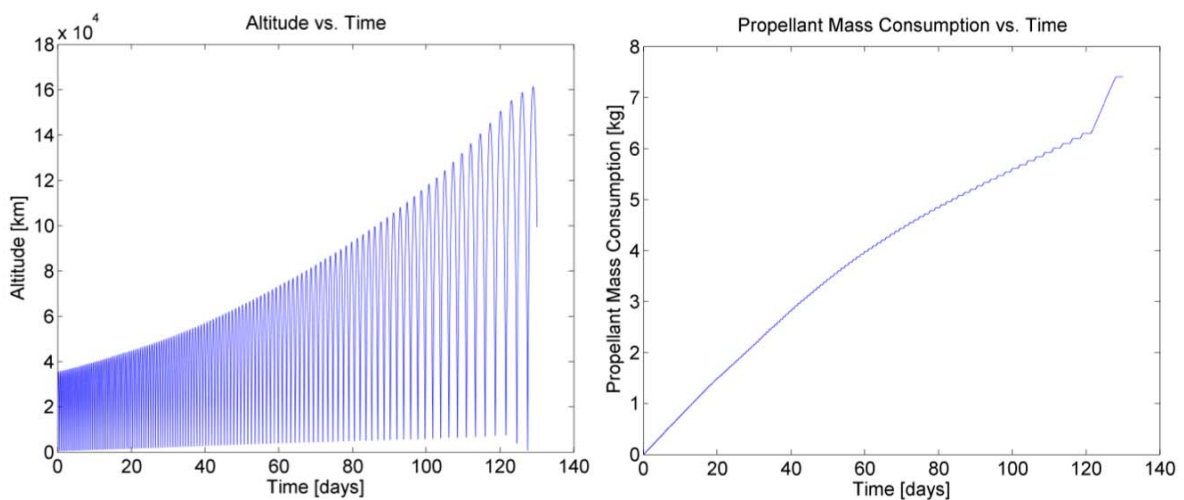


Figure 8: Evolution of propellant mass consumption (left) and altitude (right).

The first part of the curve in the left plot of Figure 8, where a smooth non-linear growth of the consumed propellant mass can be noticed, corresponds to the increase of the semi-major axis by means of phased thrusting phase. The last part of the same curve, exhibiting a quicker change in propellant mass consumption, corresponds to the eccentricity modification phase wherein the thruster operates for the entire orbit.



Figure 9 shows the time evolution of semi-major axis (top left), eccentricity (top right), Right Ascension of the Ascending Node (RAAN, bottom left) and argument of perigee (bottom right) during the transfer manoeuvre.

The first part of the top left plot of Figure 9 shows the change in the orbit semi-major axis due to the thruster firing arcs centred on the orbit perigee. During this part of the orbit transfer manoeuvre the eccentricity of the orbit (top right plot of Figure 9) is increased up to about 0.84, then the orbit eccentricity modification manoeuvre brings the spacecraft on the final target orbit. The periodic small peaks that can be noticed both in the semi-major axis and in the eccentricity plot at the end of the transfer manoeuvre phase are due to the effect of the moon gravity field on the spacecraft.

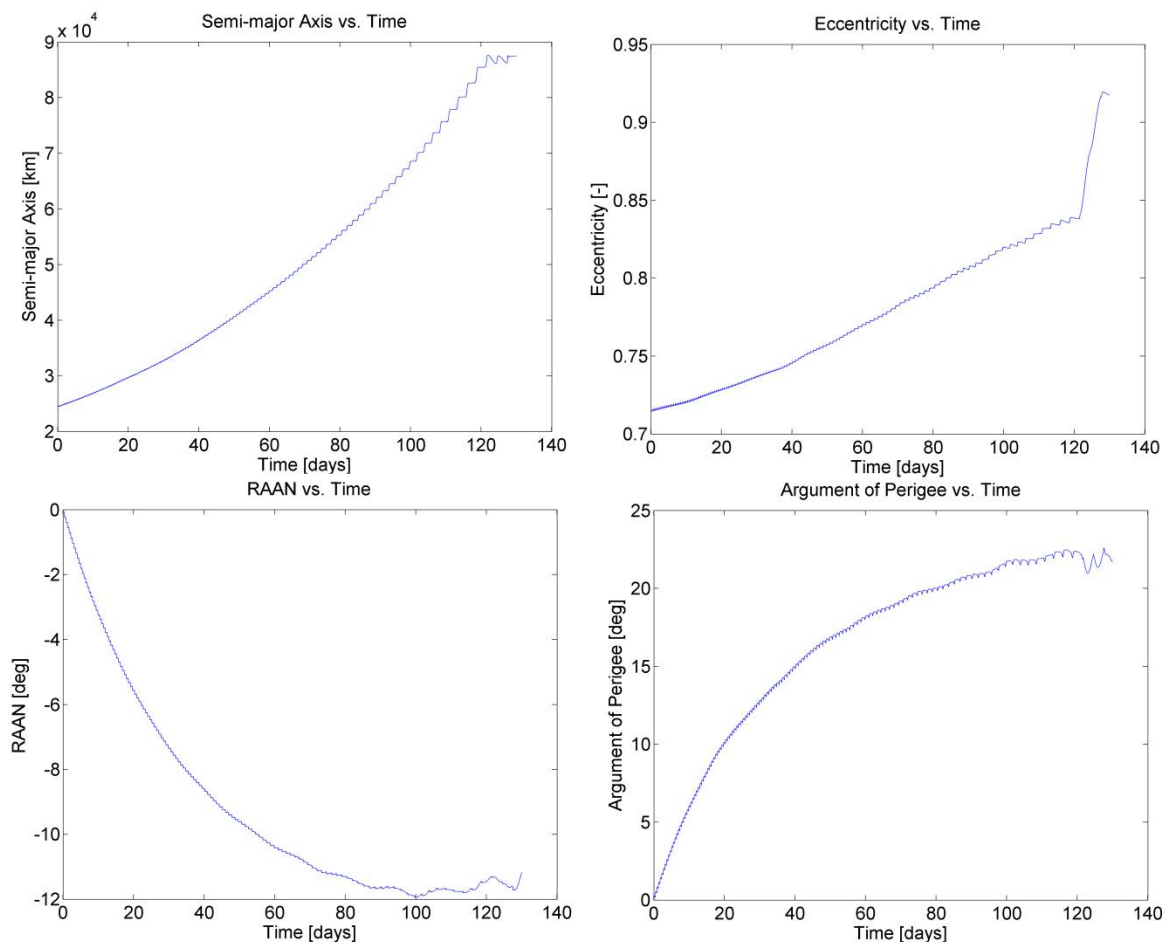


Figure 9: Evolution in time during the transfer manoeuvre of semi-major axis (top left), eccentricity (top right), Right Ascension of the Ascending Node (RAAN, bottom left) and argument of perigee (bottom right).

The RAAN and the argument of perigee of the orbit, shown respectively in the bottom left and bottom right plot of Figure 9, are relevantly changed during the transfer manoeuvre due to orbital perturbations. In particular, the final value of orbit RAAN is about -12 deg and the final orbit argument of perigee is 22 deg.

Figure 9 shows the value over mission lifetime of the incoming power (top left), spacecraft required power (top right), their difference (bottom left), and the state of charge of the batteries (bottom right).

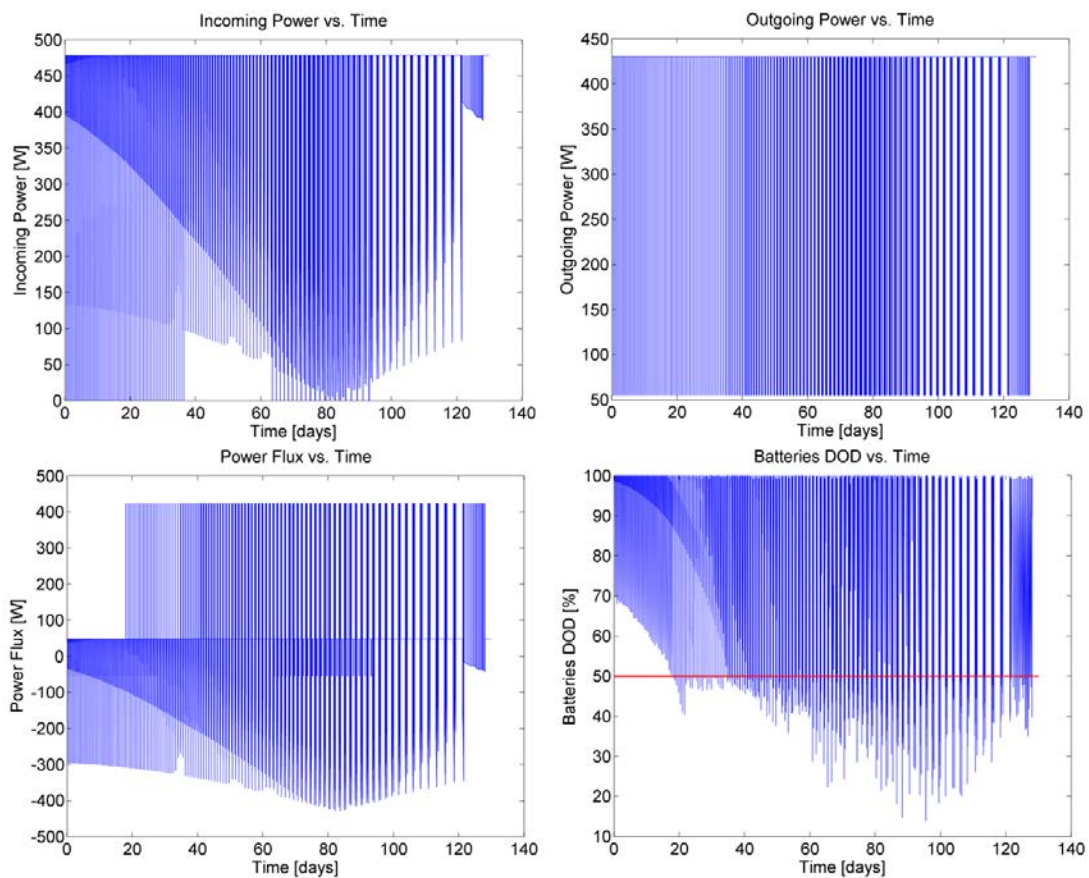


Figure 10: Value over mission lifetime of the incoming power (top left), spacecraft required power (top right), their difference (bottom left) and batteries state of charge (bottom right).

The maximum value of the power required by the spacecraft (~430 W) shown in the top right plot of Figure 9, is slightly smaller than the maximum value of the generated power (475 W, see upper left plot). However, considering the attitude constraint imposed by thrust vector direction, generated power might also be smaller than the whole amount of power required by the spacecraft

and, in this case, the energy stored in the batteries is used to enable the spacecraft to work and the thruster is switched off only when the amount of energy available in the batteries is equal to one half of maximum battery capacity. Moreover, during eclipse phases, the thruster is switched off and the energy stored in the batteries is used to enable spacecraft operations and, in particular, to operate attitude and thermal control subsystems. An accurate management of these phases, indeed, allows to immediately operating the thruster at the end of the eclipse phase reducing the overall transfer time.

To investigate the E-sail concept, one of the target orbit requirements is to have the orbital apogee outside the Earth magnetosphere. In order to do so, it is required to have the orbit semi-major axis aligned with the Sun-Earth direction at the end of the orbit transfer phase.

In first instance, it is possible to exploit the natural Earth oblateness to achieve a costless orbit perigee rotation. This approach requires some waiting time in the initial of final orbit before starting the electric transfer. Another possible approach is to realize the argument of perigee ( $\omega$ ) changing by propulsive means exploiting one or more different phasing strategies.

Table 4-3 shows the strategies that might be foreseen to fulfil the required target.

<b>Orbiting in GTO</b>	<b><math>\Delta\omega</math> [deg/day]</b>	<b><math>\Delta V</math> [m/s/day]</b>
Orbiting on GTO	1.7	N/A
Orbiting on final orbit	1.08	N/A
Thrusting on GTO	2.5	34
Thrusting on final orbit	1.8	42

Table 4-3: Natural and electric argument of perigee changing.

The argument of perigee change values listed in Table 4-3 already takes into account the relative motion of the Sun with respect to spacecraft orbit.

## 5 SUBSYSTEM PRELIMINARY DESIGN

Figures 10–12 show the spacecraft configuration conceived and the allocation of all the main subsystems within the spacecraft body. In particular, Figure 11 shows the spacecraft in the configuration with deployed solar arrays. Thermal control radiators are positioned on three sides of the spacecraft (only two of them are visible in Figure 11). The interface flange is positioned on the side of spacecraft opposite to thrusters, i.e. during launch the thruster face is direct toward the launch direction.

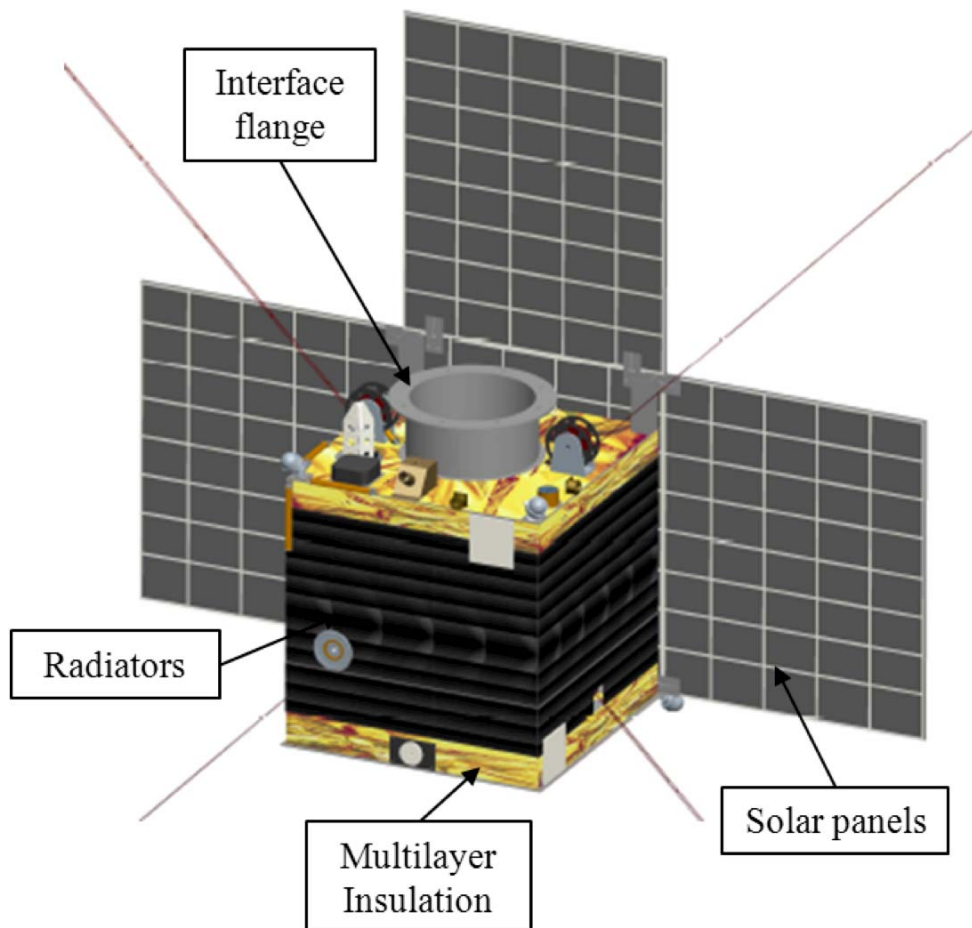


Figure 11: External view of the spacecraft in the configuration with deployed tethers and solar arrays.

Figure 12 shows the position of the reaction control wheels, of the Power Conditioning Unit (PCU), of FEEP thrusters and tethers (once released at the end of the orbit transfer phase), of the battery inside the spacecraft body and of the Primary Flight Computer and Data Recorder. Moreover, Figure 12 also shows the position of the Electron gun and of the Electron Spectrometer on the side of the spacecraft opposite to the solar panels, thus opposite to the Sun direction.

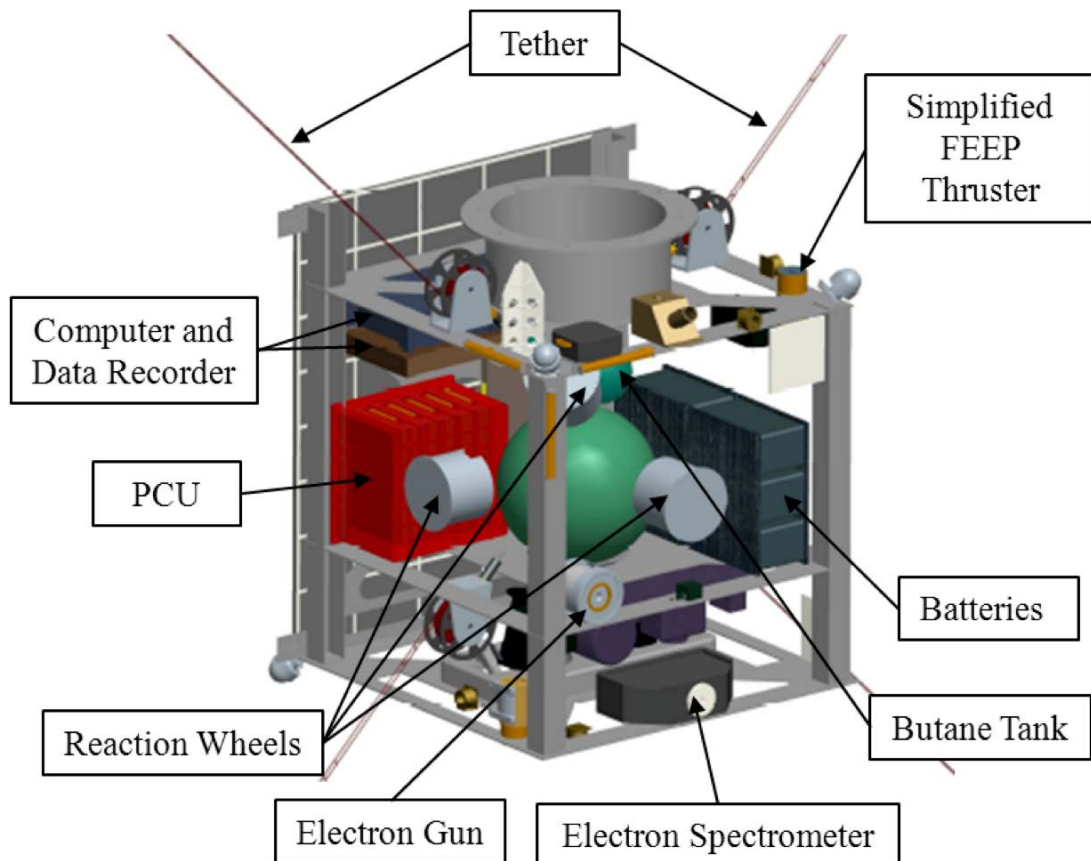


Figure 12: Internal view of the spacecraft.

Figure 13 shows all the main internal components; i.e. the position of the antennas, of three out of four Nanospace MEMS cold gas thrusters<sup>6</sup>, of the Xenon propellant tank, of the Magnetotorquers and of some sensors (Earth sensor, Sun Sensor, Accelerometer and magnetometer).

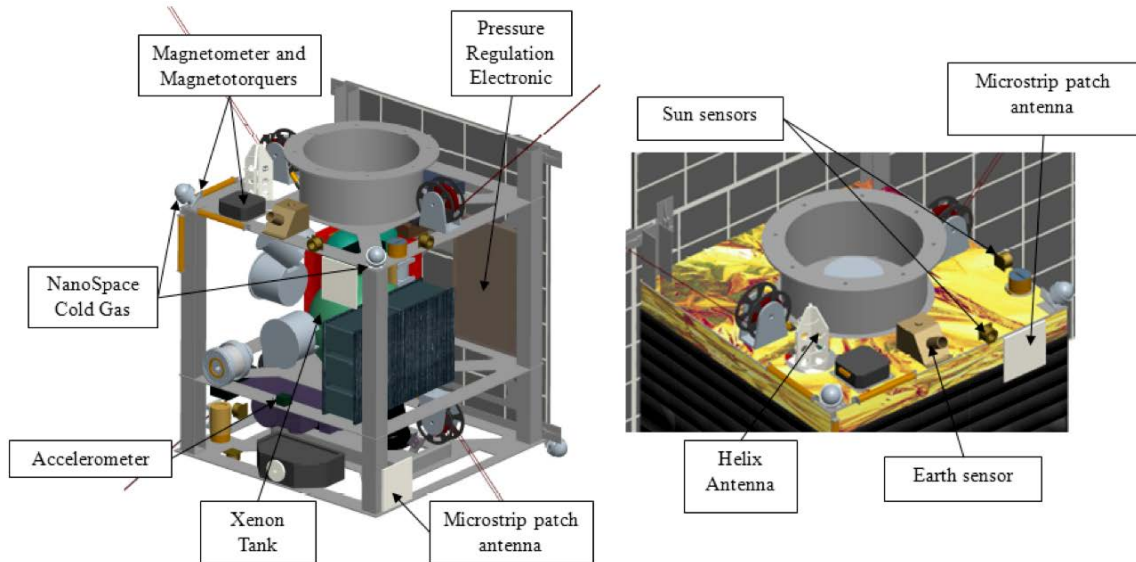


Figure 13: Internal view of the spacecraft.

Figure 14 shows the position of the two HT-400 Hall Effect Thrusters<sup>5</sup>, of the Xenon Flow Control Unit, of the Pressure Regulation Unit, of the Cold Gas thruster, of the Tether reels and of the Electron Spectrometer in the bottom part of the spacecraft.

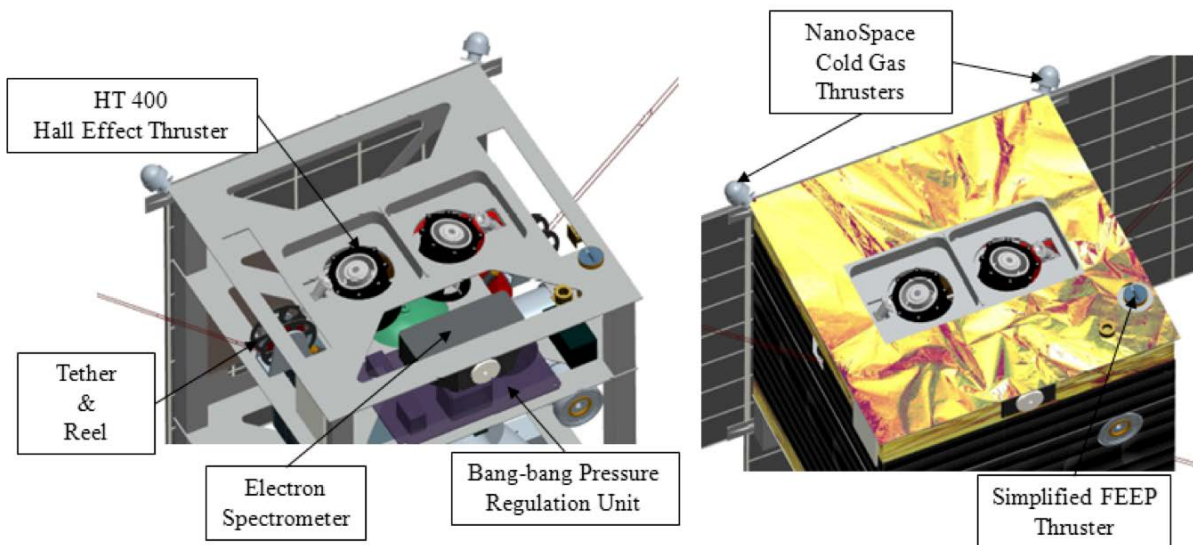


Figure 14: Internal view (left) and view (right) of the bottom side of the spacecraft.

The spacecraft mass breakdown is presented in Table 5-1.

Subsystem	[Kg]	Contingency [%]	[Kg]
Structure	6	20.0	7.2
Spacecraft Propulsion Subsystem	11.9	5.0	12.5
Payload (see Sec. 4.2)	6.2	5.0	6.5
Energy Storage Subsystem	9	5.0	9.4
Attitude and Orbit Control Subsystem	7.9	10.0	8.7
Power Generation Subsystem	6.2	10.0	6.8
Command &Data Handling	0.6	5.0	0.7
Thermal Control Subsystem	2.5	10.0	2.7
Spacecraft Communication Subsystem	2.3	5.0	2.5
<b>Total Dry Mass</b>	<b>52.6</b>		<b>57.0</b>
Xenon Propellant	8.0	2.0	8.2
<b>Total Mass</b>	<b>60.6</b>		<b>65.2</b>

Table 5-1: E-sail Demo preliminary mass breakdown.

Figure 15 shows the spacecraft mass breakdown with the mass of each subsystem expressed in percentage.

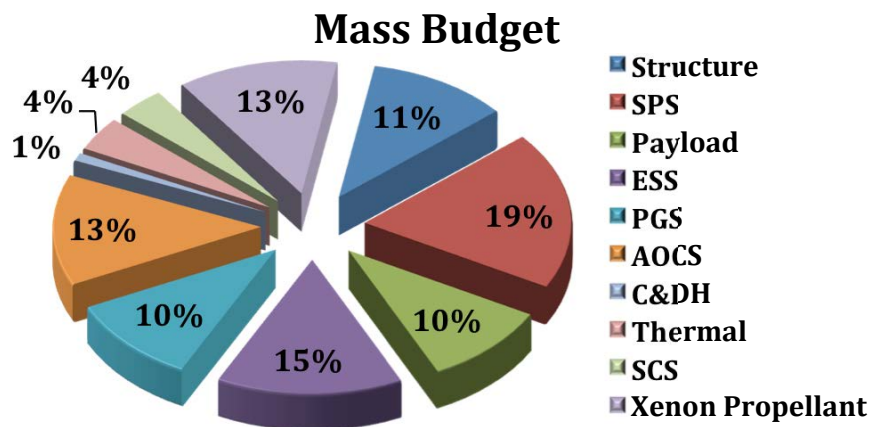


Figure 15: Spacecraft mass breakdown.

The centre of mass position has been roughly estimated considering the position of each subsystem after solar panels deployment, see Figure 16.

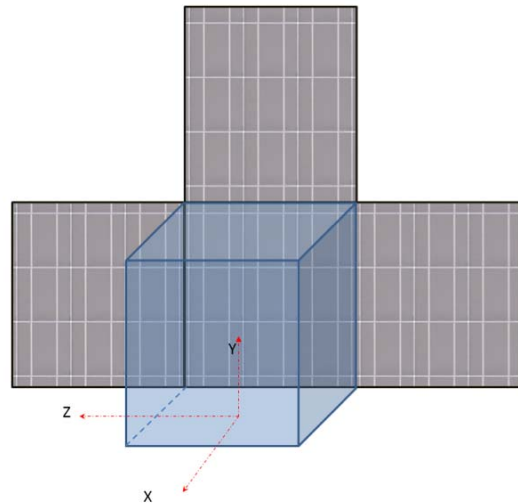


Figure 16: Schematic representation of spacecraft with the reference frame considered for the determination of centre of mass position.

Considering the reference frame represented in Figure 16, the coordinates of the centre of mass with respect to the centre of the fixation base can be computed by the preliminary spacecraft configuration. They turn out to be compliant with ASAP 5 design specifications<sup>2</sup> (in the stowed configuration) and their values are:

Configuration	$X_G$ [mm]	$Y_G$ [mm]	$Z_G$ [mm]
<b>Stowed Panels</b>	+5	388	-2.5
<b>Open Panels</b>	$-0.5 < X_G < 0.5$	372	$-0.5 < Z_G < 0.5$
<b>Complete Propellant Exhaustion</b>	$-0.5 < X_G < 0.5$	366	$-0.5 < Z_G < 0.5$

Table 5-2: Centre of Gravity position coordinates for three different mission phases.

A preliminary estimate of the values of the principal moments of inertia of the spacecraft is shown in Table 5-3.

Configuration	$J_x$ [kgm <sup>2</sup> ]	$J_y$ [kgm <sup>2</sup> ]	$J_z$ [kgm <sup>2</sup> ]
<b>Stowed</b>	4	3	3.3
<b>Open</b>	4.1	4.6	5.3

Table 5-3: Spacecraft principal Moments of Inertia.





# **E-sail Demo Preliminary Design**

Doc. No.: -  
Issue: 1.0  
Date: Nov. 20, 2011  
Page: 33 of 72

In the following sections each spacecraft subsystem is analysed and its size and mass is estimated taking into account all the main components. For each subsystem COTS components have been preferably chosen.

## 5.1 Spacecraft Propulsion Subsystem

The Spacecraft Propulsion Subsystem (SPS) is composed by two Alta's HT-400 low power Hall Effect Thrusters<sup>5</sup>, one Xenon tank, the Bang-bang Pressure Regulation Unit (BPRU), the Xenon Flow Control Unit (XFCU), the Pressure Regulation Electronics (PRE) and the Power Supply & Control Unit (PSCU). The mass of the whole system is 11.9 kg; the detailed breakdown of each component is given in Table 5-4.

Component	n°	[Kg]
<b>HT-400</b>	2	2
<b>Xenon Tank</b>	1	3.4
<b>BPRU</b>	1	1
<b>XFCU</b>	1	0.5
<b>PRE</b>	1	0.5
<b>PSCU</b>	1	4.5
<b>Total SPS</b>		<b>11.9</b>

Table 5-4: Propulsion subsystems mass breakdown.

Alta's HT-400 is a low power Hall Effect Thruster. The thruster magnetic system is based on permanent magnets and it is able to operate between 200 to 1000 W reaching a maximum specific impulse of 1780 s at 50% efficiency.

Table 5-5 shows thruster performance at the selected working point.

<b>Alta HT-400 Hall Effect Thruster</b>	
<b>Thrust [mN]</b>	25
<b>Specific Impulse [s]</b>	1250
<b>Efficiency</b>	41
<b>Power [W]</b>	375
<b>Thruster lifetime [hr]</b>	2500
<b>Mass [kg]</b>	1
<b>Dimensions [mm]</b>	φ 110x110




Table 5-5: Alta's HT-400 specifications<sup>5</sup>.

The working point selected corresponds to a maximum power requirement of 375 W with an average efficiency of about 41%. The two thrusters are supposed to be placed on the bottom of the probe and just one is required to complete the whole transfer while the other is include for cold redundancy.

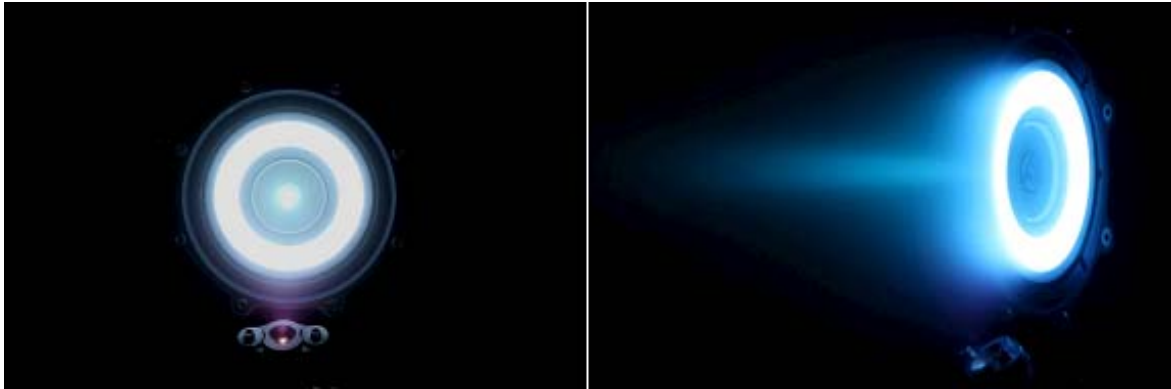


Figure 17: Alta HT-400 firing during the tests carried out in the Alta's IV4 Vacuum Chamber.

The propellant (Xenon) mass required for the transfer manoeuvre is about 7.5 kg, corresponding to 12.4% of the spacecraft initial mass.

Thrusters are mounted so as to have the thrust vector on the spacecraft Y-Z plane (see Figure 16), inclined with respect to Y axis. Figure 18 shows the plasma plume of the HT-400 Hall Effect Thruster.

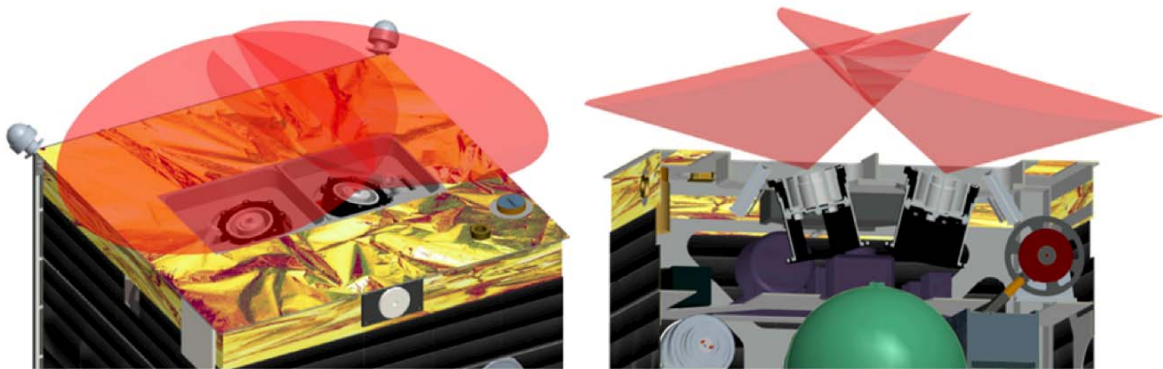


Figure 18: HT-400 Hall Effect Thruster plasma plume.

The feeding system for the thruster unit is composed by a number of sub-components requires to command and control the propulsion subsystem. Each component will be analysed in the following subsections.

## 5.2 Xenon Propellant Tank

The xenon propellant tank considered is the ATK Space Systems 80345-1, a 6.55 l monolithic titanium pressurant tank<sup>7</sup>. Considering the propellant mass and the xenon density (1.7 kg/l) at the storage pressure considered (150 bar), one tank is sufficient to store all the propellant required.

<b>ATK Space Systems 80326-1 Monolithic Titanium Tank</b>	
<b>Operating Pressure [bar]</b>	310
<b>Proof Pressure [bar]</b>	465
<b>Cryo Proof Pressure [bar]</b>	551
<b>Burst Pressure [bar]</b>	620
<b>Total Volume [l]</b>	6.55
<b>Mass [kg]</b>	3.36
<b>Heritage: DMSP / TIROS</b>	

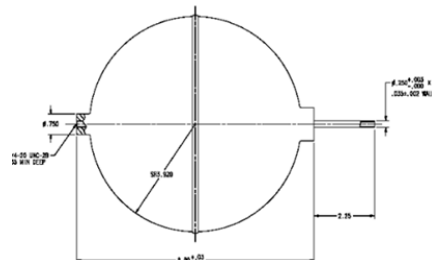


Table 5-6: ATK Space Systems 80326-1 Monolithic Titanium Tank specifications.

## 5.3 Bang-bang Pressure Regulation Unit

The Bang-bang Pressure Regulation Unit (BPRU) relies on the use of valves in bang-bang mode. Instead of using the valves with the classical concept of Pulse Width Modulation (PWM), the concept chosen for the system is to use an intermediate small volume for the transfer of a small quantity of gas from the high pressure tank, and then after a certain time step, release that quantity of gas toward a plenum volume. This intrinsic concept of Bang-Bang regulator introduce a very regular fluctuation of the “constant regulated pressure”: each time the plenum measured pressure becomes lower than the target pressure, the bang-bang valves are activated and a small positive step in the pressure of the plenum volume occurs. Xenon from the tank is delivered to the BPRU. Filters are necessary to assure the cleanliness of the gas before bang-bang valves.

## 5.4 Xenon Flow Control unit

The Xenon Flow Control (XFC) unit has the task to feed anode and cathode with fixed mass flow rate. In particular the level of flow depends on the command from PSCU that directly control the thruster. The XFC selected is an Ampac Marotta UK Ltd SP05 Xenon Flow Control Unit. It has a mass of 0.5 kg and its maximum dimensions are 128x79x25 mm<sup>8</sup>.

**Ampac Marotta UK Ltd SP05 Xenon Flow Control Unit**

<b>Anode Flow Rates [mg/s]</b>	4.7 – 8.5
<b>Cathode Flow Rates [mg/s]</b>	0.3 – 0.6
<b>Total Flow Rates [mg/s]</b>	5 - 9
<b>Dimensions [mm]</b>	128x79x42
<b>Operating Temperature [°C]</b>	-40°C to
<b>Mass [kg]</b>	<0.5
<b>Heritage:</b>	Qualified for ROS2000 thruster

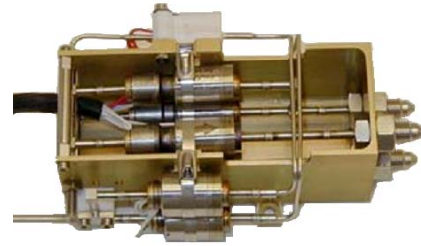


Table 5-7: Ampac Marotta UK Ltd SP05 Xenon Flow Control Unit specifications.

## 5.5 Pressure Regulation Electronics

The Pressure Regulation Electronics (PRE) card fully controls and supply power to one of the bang-bang valves of the BPRU in absolute sequential operational procedure. In addition, it prevents simultaneous operation of the upstream and downstream valves of a single branch. The electronic regulator conceived is composed of two electromechanical valves in series, with a high pressure gas supply upstream and three pressure transducers downstream. A free volume exists between the two valves. A controller receives input from the pressure transducers and drives the valves to meet downstream pressure requirements.

## 5.6 Power Supply & Control Unit

The Power Supply & Control Unit (PSCU) is in charge of monitoring and controlling the PGS, the ESS and all the other power requirements switching individual subsystems either in response to a remote command or automatically in case of an overload or of short-circuit condition. Moreover, it integrates the pressure regulation unit electronics. The PSCU also provides interfaces to the spacecraft telemetry. Part of this unit is analysed in Sec.5.14.

The PSCU is based on a modular structure, presently being developed on the basis of existing switching power converters. The mass of PSCU is estimated at about 4.5 kg.

## 5.7 Payload

The satellite payload is composed of two pairs of reels, each one equipped with 1 km of conductive tethers, an imaging system, an electron gun, plus the thrust diagnostics and all the environmental sensors required to characterize the local conditions of the solar wind. The two ionic liquid FEED<sup>10</sup> thrusters, mounted on the top and bottom surface, are necessary to provide to the satellite the spin required to deploy the four tethers.

The payload is assumed to operate for approximately 3 months after the end of the orbit transfer phase. During payload operation phase, one electron spectrometer will be used to measure the solar wind electron flux on the spacecraft and one 3W 20kV Electron Gun will be operated to modify spacecraft and tethers potential with respect to the external solar wind. The thrust exerted by the solar wind on the spacecraft will be measured by means of four Colibrys SF 1500 accelerometers.

The mass of each component and of the whole payload is listed in Table 5-8.

<b>Payload</b>	<b>Mass [kg]</b>
<b>Tether</b>	<0.1
<b>FEED</b>	1.6
<b>Tether Imaging System</b>	0.5
<b>Reel &amp; Stepper Motors</b>	1.6
<b>Electron Spectrometer</b>	1.0
<b>High Voltage Subsystem</b>	1
<b>Electron Gun</b>	0.3
<b>Accelerometer</b>	0.1
<b>Payload Total Mass</b>	<b>6.2</b>

Table 5-8: Payload mass breakdown

## 5.8 Alta Simplified FEED Thruster

Two oppositely mounted Alta Simplified FEED thruster will be used to provide to the spacecraft the initial spin up at the beginning of payload operation phase. The total mass considered for each thruster unit (800 g) includes the mass of the required propellant and electronics. Table 5-9 shows the Alta Simplified FEED thruster<sup>10</sup> specifications.

<b>Alta Simplified FEEP thruster</b>	
<b>Thruster range [mN]</b>	50 - 200
<b>Specific impulse [s]</b>	2000
<b>Power [W]</b>	4
<b>Diameter [mm]</b>	60
<b>Height [mm]</b>	70
<b>Dry Mass [g]</b>	155

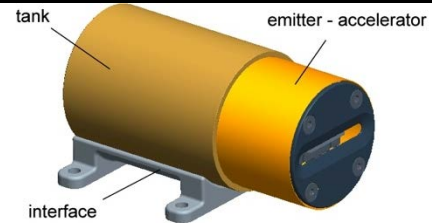


Table 5-9: Alta Simplified FEEP thruster specifications.

Figure 19 shows the plume of Simplified FEEP and cold gas thrusters with respect to the body of the spacecraft.

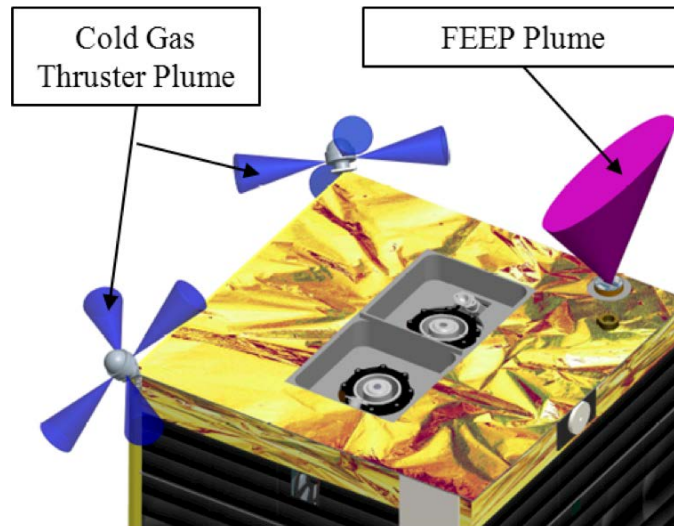


Figure 19: FEEP and Cold Gas thruster plumes with respect to spacecraft.

The thruster arrangement and the general probe layout assures the minimum interaction of the thruster plumes with the spacecraft surfaces and with the other thruster units.

## 5.9 Tethers and Reel Mechanism

Four reel mechanisms are required to deploy and control the tethers. Each tether reel is capable of holding a 9 mm wide Hoytether. It is composed by a tether box with a bearing release system and a stepper motor to control the deployment. A small mass (of the order of few tens of grams) is fixed

on the tip of each tether to enable its deployment during satellite rotation<sup>1</sup>. Each tether is assumed to weight 25 g and 0.4 kg are assumed for the each reel and associated stepper motor.

In total the tether release mechanism is estimated to weight 1.7 kg.



Figure 20: Schematic representation of the tether release mechanism with tether, reel and stepper motor.

## 5.10 Tether Imaging System

The purpose of the tether imaging system is to verify the deployment of the tethers and to determine the coordinates of the tether end mass. This system will be developed within the SWEST project by Tartu Observatory. The imaging system will be composed of 4 identical camera modules pointed in the direction of tether deployment and a central image processor.

The central processor might be implemented as a separate FPGA (Field-Programmable Gate Array) in the CDHS system or a powerful ARM processor such as the STM32F217ZGT6. This processor will gather the images from the camera modules and store them in the main data recorder. It will also do image processing in order to determine the coordinates of the tethers.

The camera modules will consist of small low power ARM processor to interface with the sensor, the memory and the central processor. Both the sensor and memory use parallel interfaces for data transfers and during image acquisition DMA (Direct Memory Access) can be used. Communication between the camera modules and the central processor will use a serial interface such as CAN (Controller Area Network). The memory will have to be fast and big enough to store one image during image acquisition.



For the image sensor a larger radiation tolerant sensor like the STAR1000 by On Semiconductor could be used, however the resolution might be too small and the sensor dimensions too large. Hence it will be necessary to test some smaller sensors that are not specifically radiation tolerant. Since only brightness is required to determine the location of the tether end mass, a monochromatic sensor can be used.

For the lens a commercially available off the shelf lens, like a Megapixel Finite Conjugate Micro Video Lens by Edmund Optics, can be used. The lens has to be able to capture the end mass both when it is close to the spacecraft and when it is fully deployed. Given that the spacecraft is spinning during tether deployment, the end mass will be relatively stationary compared to the background. Also the end mass is brighter than the stars in the background. So a longer exposure times can be used to overexpose the end mass and allow the stars to move, which will make detection easier. Radiation shielding is required for the main electronics components (processors and memory).

<b>Tether Imaging System</b>	
<b>Peak Power [W]</b>	1
<b>Mass [kg]</b>	0.5
<b>Operating Temperature [°C]</b>	-30 to +70
<b>Resolution [Mpixels]</b>	2
<b>Data per image [Mb]</b>	2.3

Table 5-10: Tether imaging system specifications.

## 5.11 Colibrys SF 1500 Accelerometer

Four accelerometers<sup>11</sup> are required to measure the effect of the solar wind on the electric sail and on the spacecraft. The Colibrys SF 1500 series is chosen as reference; its main data are summarized in Tab. 4-13.

<b>Colibrys SF 1500 Accelerometer</b>	
<b>Output Range [g]</b>	±3
<b>Noise Level [<math>\mu\text{g}_{\text{rms}}/\sqrt{\text{Hz}}</math>]</b>	0.3
<b>Sensitivity [V/g]</b>	1.2 ± 0.12
<b>Dimensions [mm]</b>	25 x 25 x 16
<b>Operational Temperature [°C]</b>	-40 to +85
<b>Mass [g]</b>	6.7



	<b>E-sail Demo Preliminary Design</b>	Doc. No.: - Issue: 1.0 Date: Nov. 20, 2011 Page: 42 of 72
---	---	--

---

**Heritage:**

---

Table 5-11: Colibrys SF 1500 Accelerometer specifications.

## 5.12 High-voltage Subsystem

The purpose of the high-voltage (HV) subsystem (Univ. Jyväskylä) is to allow biasing any or all of the four tethers to the wanted 0-20 kV positive potential with respect to distant space plasma. The HV subsystem uses electron guns for pumping out negative charge from the system so that positive biasing can occur. The electron guns are connected to an internal HV bus which is a conducting cable inside the spacecraft, electrically insulated from the spacecraft chassis. Each gun has its own dedicated HV source. Some guns (“mode A”) are connected to the HV bus by their cathode and some (“mode B”) by their anode. The mode A guns act effectively as electron emitters that prevent the HV bus from going significantly negative with respect to space plasma, regardless of tether potential and tether current. In contrast, using mode B guns the HV bus can be raised to a high positive potential with respect to space plasma. Each tether is connected to the HV bus through its own dedicated HV source that can bias the tether 0-20 kV positive with respect to the HV bus. No HV switches are needed in this design and there is a large amount of redundancy which protects us against HV power source failures. Each gun has a control grid for regulating the produced current independently from the voltage setting. The baseline for the HV source (all sources of the same type) is EMCO DX-series<sup>12</sup> unit with NASA approved ASTM E595-93 low outgassing epoxy option.

The baseline for the electron guns is traditional heated cathode. Cold cathode solutions are considered as an option. Cold cathode electron guns built in Jyväskylä will fly with the ESTCube-1 and Aalto-1 CubeSat E-sail test missions in 2012 and 2013, respectively.

## 5.13 Power generation Subsystem

The Power Generation Subsystem (PGS) is in charge of producing energy during all mission phases by means of four triple junction GaAs/Ge solar arrays. One body-mounted solar panel is initially overlapped with one deployable solar panel that is opened during first mission phases. At the same time, other two deployable solar panels, initially stowed over spacecraft sides, are deployed reaching a total area of about  $1.7 \text{ m}^2$ , see Figure 21. The total power generated by the solar panels is about 478 W at the beginning of life and, considering a state-of-the-art value for the power-to-mass ratio of 77 W/kg, their mass is estimated to be about 6.21 kg.

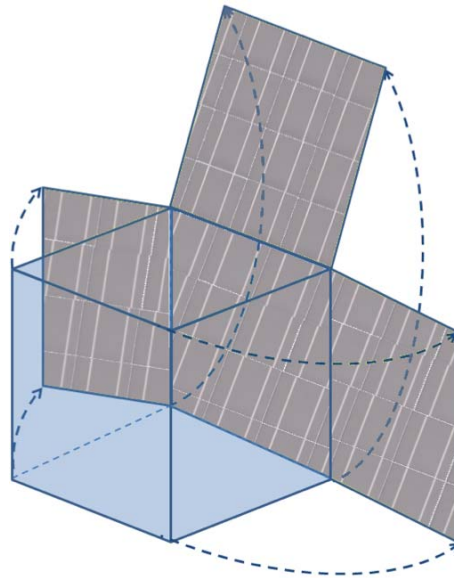


Figure 21: Schematic representation of solar panels deployment.

### 5.13.1 PGS Preliminary Sizing

The preliminary sizing of the PGS is carried out considering commercial space proven solar cells currently available from the three leading cells suppliers (AzurSpace, Emcore, Spectrolab).

Table 5-12 shows the most relevant cells characteristics for the cell models of interest.

<b>Producer &amp; Name</b>	<b>Efficiency [%]</b>	<b>Size [mm]</b>	<b>Area [cm<sup>2</sup>]</b>	<b>Weight [g/cm<sup>2</sup>]</b>
<b>Emcore ATJ</b>	27.5	40x80	30.18	0.084
<b>Emcore ZTJ</b>	29.5	40x80	30.18	0.084
<b>Emcore TJM</b>	27.0	40x80	30.18	0.084
<b>Emcore BTJ</b>	28.5	40x80	30.18	0.084
<b>Emcore BTJM</b>	28.0	40x80	30.18	0.084
<b>AzurSpace 3G27</b>	27.0	40x80	30.18	0.086
<b>AzurSpace 3G28</b>	28.0	40x80	30.18	0.086
<b>AzurSpace 3G30C</b>	29.1	40x80	30.18	0.086
<b>Spectrolab UTJ</b>	28.6	80x80	59.65	0.084
<b>Spectrolab ITJ</b>	26.5	40x80	31.00	0.084
<b>Spectrolab XTJ</b>	29.3	80x80	59.65	0.084

Table 5-12: Most relevant characteristics of AzurSpace, Emcore and Spectrolab space proven solar cells.

Considering the size of the spacecraft solar panels (600x710 mm) and the average size of the considered cells, a maximum of 14 rows and 8 columns of cells can be positioned on each array. Thus, the spacecraft can be equipped with a total of 448 solar cells that, considering a conservative efficiency value of 26% (the minimum for triple junction solar cells) and a cell area of 30.18 cm<sup>2</sup>, would provide a maximum of 478 W at the begin of life.

## 5.14 Energy Storage Subsystem

The Energy Storage Subsystem (ESS) is in charge of storing the energy produced by solar arrays during all mission phases and it is composed by the batteries, the Battery Charge Regulator (BCR) Module and the Power Conditioning Module (PCM).

The ESS subsystem is based on Li-Ion MicroSat SAFT battery<sup>4</sup>. Its mass is about 4.50 kg and its dimensions are 220x170x95 mm. In order to provide redundancy to the subsystem, the spacecraft will be equipped with two identical SAFT battery packs, one for cold redundancy.

Table 5-13 shows the most relevant characteristic of SAFT Micro Li-Ion<sup>4</sup> battery pack.

<b>SAFT Li-Ion MicroSat Battery Pack</b>	
<b>Nominal energy [Wh]</b>	480
<b>Nominal capacity [Ah]</b>	16.8
<b>Battery EOCV [V]</b>	32.8
<b>Width [mm]</b>	220
<b>Length [mm]</b>	170
<b>Height [mm]</b>	95
<b>Mass [kg]</b>	4.5
<b>Heritage:</b> SSETI, Proba 2, Rasat, Agile	



Table 5-13: Most relevant characteristic of SAFT MicroSat Li-Ion Battery Pack.

Considering the spacecraft power consumption during eclipse phases (55 W) and the battery nominal energy storage capability (475 Wh), more than 8 hours of autonomous of spacecraft operation can be provided (from the preliminary mission analysis, it has been determined that the maximum eclipse duration for the considered transfer manoeuvre is about 4 hours).

The BCR Module and the PCM provide interfaces to the solar arrays and. The BCR is also in charge of controlling the energy stored in the batteries during sunlight and eclipse periods. Both BCR and PCM are included in the PSCU unit described in Sec. 4.1.4.

## 5.15 Attitude and orbit control Subsystem

The Attitude and Orbit Control Subsystem (AOCS) is preliminarily designed considering space proven COTS components. The system is composed by four RW 90 Astro-und Feinwerktechnik reaction wheels<sup>13</sup> mounted in a tetrahedral configuration to obtain a 3-zero axis bias control. The desaturation of the reaction wheels is performed by means of 4 MEMS cold gas thrusters (see Sec.

5.7) placed on the top and the bottom side of the spacecraft symmetrically placed with respect to the centre of mass; see Figure 22.

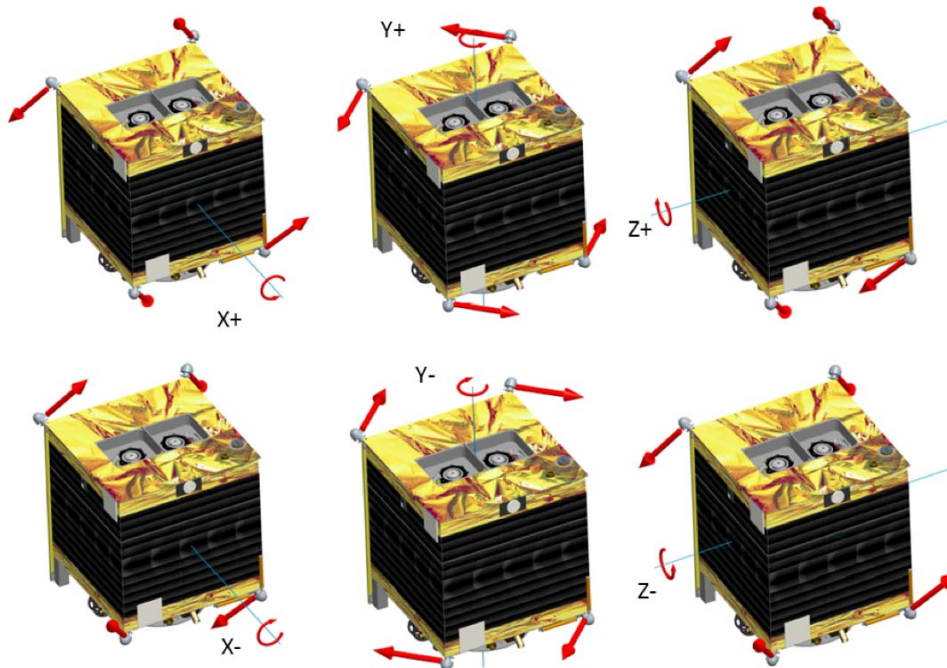


Figure 22: Torques generated by the Cold Gas thrusters for the desaturation of the reaction wheels.

Three ZARM Technik Magnetic Torquers<sup>14</sup> have been also included for redundancy in case cold gas thrusters are not able to perform reaction wheels desaturation. Moreover, four SSBV Fine Sun Sensors<sup>15</sup>, one ZARM Technik magnetometer<sup>16</sup> and one SSBV Earth Horizon Sensor have been included. Table 5-14 shows the AOCS mass breakdown.

AOCS	n°	[kg]
AOCS Electronics	1	0.25
Earth Horizon Sensor	1	0.5
Sun sensors	4	0.1
Cold Gas		0.4
Butane Propellant		1.2
Butane Tank		1.5
Magnetotorquers	4	0.3
Magnetometers	1	0.05
Reaction wheels	4	3.6
<b>Total AOCS</b>		<b>7.9</b>

Table 5-14: AOCS mass breakdown.

The most relevant properties of Astro- und Feinwerktechnik Adlershof GmbH RW90 reaction wheels<sup>13</sup> are listed in Table 5-15.

<b>Reaction Wheel: RW 90 Astro – und Feinwerktechnik</b>	
<b>Diameter [mm]</b>	103
<b>Height [mm]</b>	80
<b>Mass [g]</b>	900
<b>Angular momentum [Nms]</b>	0,34
<b>Operational Speed Range [rpm]</b>	6000
<b>Nominal reaction Torque [mNm]</b>	15
<b>Operating temperature [°C]</b>	-20/50
<b>Heritage:</b> Bird	



Table 5-15: Astro – und Feinwerktechnik reaction RW90 wheels specifications.

### 5.15.1 Attitude Sensors

Four Fine Sun Sensors have been included to achieve full sky coverage and determine spacecraft body attitude with respect to the Sun.

<b>SSBV Fine Sun Sensor</b>	
<b>Field of view</b>	140°
<b>Average Power Consumption [mW]</b>	210
<b>Peak Power Consumption [mW]</b>	728
<b>Size [mm]</b>	34x32x21
<b>Mass [g]</b>	35
<b>Heritage:</b> 14 on-orbit sensors on 4 LEO satellites	



Table 5-16: SSBV Fine Sun Sensor specifications

One SSBV Earth Horizon Sensor is also included to sense the attitude of the spacecraft. It becomes the primary attitude sensor during eclipse phases. Table 5-17 shows the sensor specifications.

<b>SSBV Earth Horizon Sensor</b>	
<b>Field of view</b>	±5°
<b>Peak Power Consumption [W]</b>	1.5
<b>Peak Power Consumption [mW]</b>	728
<b>Size [mm]</b>	61x95x61
<b>Mass [g]</b>	500
<b>Heritage:</b> TOPSAT, Orbcomm 2 <sup>nd</sup> Generation & Quicksat	



Table 5-17: SSBV Earth Horizon Sensor specifications.

One ZARM Technik AMR digital Magnetometer is also included, on the external face of the spacecraft to measure the external magnetic field for the assessment of the torque to be applied by the Magnetic Torquers. Table 5-18 shows the magnetometer specifications.

<b>ZARM Technik AMR digital Magnetometer</b>	
<b>Field range [<math>\mu\text{T}</math>]</b>	±250
<b>Scale factor [<math>\mu\text{T/bit}</math>]</b>	10
<b>Power consumption [W]</b>	0.6
<b>Size [mm]</b>	56x36x17
<b>Mass [g]</b>	55



Table 5-18: ZARM Technik AMR digital Magnetometer specifications.

Figure 23 shows the fields of view of the Earth and Sun sensors.

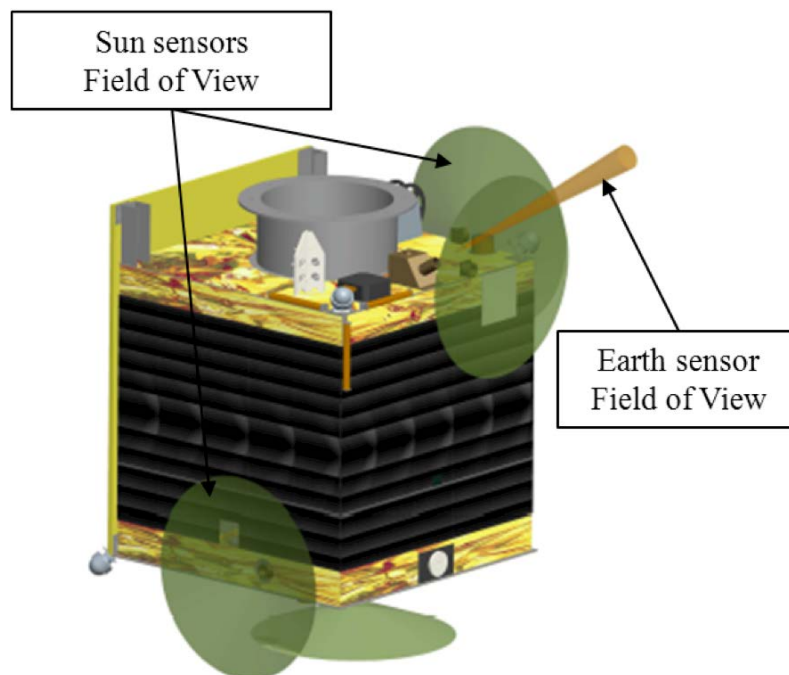


Figure 23: Field of View of the Earth sensor (orange) and of the four Sun sensors (green).

With the assumed configuration of these sensors the spacecraft is able to acquire the Sun direction in each possible attitude configuration.



### 5.15.2 NanoSpace MEMS Cold Gas Thruster

Two pairs of NanoSpace MEMS cold gas thrusters, already used for the desaturation of the reaction wheels, will be also used to give to the spacecraft the initial spin up at the beginning of payload operation phase in case of failure of Simplified FEED system. Table 5-19 shows the most relevant characteristics of the NanoSpace cold gas thruster 6.

NanoSpace Cold Gas Thruster	
<b>Thruster range [mN]</b>	0,01 - 1
<b>Specific impulse [s]</b>	50 - 75
<b>Required Power [W]</b>	2
<b>Operating temperature [°C]</b>	0 - 50
<b>Operating pressure [bar]</b>	4
<b>Diameter [mm]</b>	44
<b>Height [mm]</b>	51
<b>Mass [g]</b>	115
<b>Heritage: PRISMA</b>	



Table 5-19: NanoSpace Cold gas thruster specifications.

### 5.15.3 Liquid Butane Propellant Tank

Considering the density of liquid butane ( $0.6 \text{ kg/dm}^3$  @0 °C, 1 atm) and the propellant mass required for the desaturation of the reaction wheels with a 20% margin, the required tank volume is estimated to be about  $1.25 \text{ dm}^3$ . One AMPAC BS25-001 stainless steel propellant tank has been considered for liquid butane storage. Table 5-20 shows the AMPAC BS25-001 stainless steel propellant tank specifications.

AMPAC BS25-001 stainless steel propellant tank	
<b>Operating Pressure [bar]</b>	4
<b>Max Capacity [l]</b>	2.5
<b>Length [mm]</b>	326
<b>Diameter [mm]</b>	114
<b>Operational Temperature [°C]</b>	-40 to +65
<b>Mass [kg]</b>	1.5
<b>Heritage: NigeriaSat-1, AlSat-1</b>	



Table 5-20: AMPAC BS25-001 stainless steel propellant tank specifications.

## 5.15.4 Reaction Wheels Desaturation Propellant Mass Estimation

The estimation of the propellant mass required to perform the desaturation of reaction wheels during the whole spacecraft life is carried out under the following simplifying assumptions:

1. Torques considered in the present analysis are due to atmospheric drag, solar radiation pressure, gravity gradient and Earth magnetic field.
2. All external torques act at the same time on one single axis.
3. Only 2 cold gas thrusters are in charge of performing reaction wheels desaturation.
4. All external torques are estimated conservatively as constant and equal to the maximum predictable value.

In particular, the torque due to the misalignment of atmospheric drag centre of pressure and the spacecraft centre of mass is estimated considering the maximum spacecraft drag exposed area ( $1.26 \text{ m}^2$ ), the maximum spacecraft relative velocity at the perigee of the final orbit ( $\sim 10.5 \text{ km/s}$ ) and the atmospheric density at the perigee altitude ( $8 \cdot 10^{-14} \text{ kg/m}^3$ ). Assuming a maximum value for the distance between atmospheric drag centre of pressure and spacecraft centre of mass of 10 cm, the resulting atmospheric drag torque is about  $1.22 \cdot 10^{-6} \text{ Nm}$ .

The torque due to interaction between spacecraft magnetic dipole and Earth magnetic field is assessed considering the intensity of Earth magnetic field by means of a first order dipole model ( $5.3 \cdot 10^{-5} \text{ T}$ ). Spacecraft magnetic properties have been estimated assuming that the dipole moment for unit mass of the spacecraft<sup>18</sup> is  $10^{-3}$ , thus the resulting maximum magnetic torque is  $2.8 \cdot 10^{-6} \text{ Nm}$ .

The torque due to solar radiation pressure is estimated, similarly to the atmospheric drag torque, assuming a maximum value for the distance between solar radiation centre of pressure and spacecraft centre of mass of 10 cm and a maximum spacecraft solar radiation pressure exposed area of  $1.26 \text{ m}^2$ . The resulting torque is about  $5.68 \cdot 10^{-7} \text{ Nm}$ .

The torque due to gravity gradient is estimated considering the values of spacecraft moments of inertia derived from the preliminary spacecraft configuration (see Table 5-3). The resulting torque, assuming a maximum error of 45 deg on attitude angles, is about  $1.24 \cdot 10^{-6} \text{ Nm}$ .

The torque due to thrust misalignment can be assessed considering the thrust exerted on the spacecraft during thruster operation (25 mN), the ratio between firing time ( $\sim 1083$  hours) and total mission time and the torque lever ( $\sim 1 \text{ mm}$ ) obtained considering the maximum centre of gravity

displacement and the thrusters inclination with respect to spacecraft Y axis (see Figure 18). The torque resulting from the thrust misalignment is about  $3.8 \cdot 10^{-6}$  Nm.

Summing up all contributions, the total torque due to the considered perturbation is about  $9.9 \cdot 10^{-6}$  Nm. Considering the maximum angular momentum that can be stored by the reaction wheels chosen (0.1 Nms), about 2.8 hours are sufficient to saturate each wheel. This duration corresponds to 26% the orbital period of the initial orbit and 4% the final orbit period. Considering the thrust exerted by 2 couples of cold gas thrusters operating at the same time and their relative position (including their angular offset), the torque that can be exerted to enable the desaturation of the reaction wheels is about  $6e-4$  Nm. Accordingly, about 166 s of cold gas thrusters operation and 45 mg of propellant are required to desaturate the reaction wheels. Considering a total mission time of 5232 hours, corresponding to 128 days of orbit transfer and 3 months of payload operation, the desaturation of reaction wheels has to be performed about 1864 times with a corresponding total propellant consumption of about 1.2 kg. An additional 20% margin has been included in the mass budget for contingency.

### 5.15.5 Magnetic Torquers

Three ZARM Technik MT 1-1 Magnetic Torquers<sup>14</sup> are included in the spacecraft in order to enable a relevant propellant saving for the desaturation of the reaction wheels. Moreover, they can also operate as partial backup in case of cold gas thrusters failure.

<b>ZARM Technik MT 1-1 Magnetic Torquers</b>	
<b>Magnetic dipole [Am<sup>2</sup>]</b>	±1
<b>Power [mW]</b>	230
<b>Mass [g]</b>	60
<b>Length [mm]</b>	132
<b>Diameter [mm]</b>	13,5



Table 5-21: ZARM Technik MT 1-1 Magnetic Torquers specifications.

Under the same assumptions listed in Sec. 5.15.4 and considering a value of  $2.29 \cdot 10^{-5}$  T for the Earth magnetic field intensity at perigee, the total magnetic torque that can be exerted by one Magnetic Torquer is about  $2.29 \cdot 10^{-5}$  Nm. Accordingly, the time required for the desaturation of the reaction wheels with the considered Magnetic Torquers is about 1.21 hours.

## 5.16 Command and Data Handling System (CDHS)

The command and data handling system (CDHS) will be developed within the SWEST project as a collaboration between FMI and Tartu Observatory. The spacecraft's main computer will be a simple processor which is implemented on a commercial FPGA (Field-Programmable Gate Array) chip. FMI has extensive experience in building FPGA-based data processing units and computers on various space instruments, for example the ASPERA charged particle detectors on the ESA Mars Express and Venus Express planetary missions, the SPEDE instrument on SMART-1 and LAP and ICA on the Rosetta orbiter. The processing power requirements of SWEST are small which enables us to use a relatively inexpensive hardware solution while achieving a sufficient level of radiation tolerance for the mission. A somewhat larger (but still moderate) processing power requirement would come from the tether imagers that must compress images and find bright objects in them. However, the baseline is to use a dedicated image processing computer (also FPGA-based) that only needs to work in the solar wind, not when traversing the radiation belts; furthermore, single event upset errors in the images are not fatal for mission success and can be tolerated to some extent. Thus the processing power requirements of the main computer (which should work always, also in the radiation belts) can be kept small. Enough (up to 1 cm) of radiation shielding can be used to protect the computer; for this reason the total allocated mass budget for the whole CDHS including processor, electronics board, memory, connectors and radiation shielding box is 0.6 kg and its characteristics are listed in Table 5-22.

CDHS	
<b>Power [W]</b>	2
<b>Mass [kg]</b>	0,6
<b>Dimensions [mm]</b>	120x170x60
<b>Operating Temperature [°C]</b>	-55 to +65

Table 5-22: CDHS characteristics.

## 5.17 Thermal control Subsystem

The Thermal Control Subsystem (TCS) shall maintain all the equipment within the temperature range applicable to all mission phases. It is designed to guarantee adequate margins between the predicted units extreme temperature ranges (based on worst design cases) and the required operational temperature limits.

For the spacecraft equipment, the temperature range listed in the Table 5-23 has been assumed.

Component	Op. Range [°C]	Non-op. Range [°C]	Design Range [°C]
<b>Electronic Units</b>	-10 to 50	-20 to +60	-10 to +50
<b>Batteries</b>	0 to +20	-5 to +25	0 to +20
<b>Magnetometer</b>	-40 to 80		
<b>Reaction wheel</b>	-20 to 50	-30 to +60	
<b>Sun sensor</b>	-25 to 50		
<b>Earth sensor</b>	-30 to 55		
<b>Cold Gas thrusters</b>	0 to 50	-60 to -10	
<b>Butane prop. system</b>	-20 to 60		
<b>Medium gain antenna</b>	-150 to 95		
<b>Low gain antenna</b>	-100 to 100		
<b>Primary computer</b>	-20 to 50		
<b>Data recorder</b>	-20 to 50	-30 to +60	

Table 5-23: Spacecraft components and relative operative and design temperature range.

The analysis is carried out considering the two main satellite heat sources: the solar flux on the surface of the satellite and the power generated by the thruster. The temperature of most of spacecraft components is meant to be controlled by means of passive thermal control methods while the most critical ones (tank, batteries) will be actively controlled.

The total area of thermal radiator is estimated under the following assumptions:

1. Albedo and earth thermal infrared flux are neglected;
2. A nominal operating temperature of 290 K is considered, with a maximum admitted variation of 10 degrees;
3. For thrusters is assumed a total efficiency of 41% so the 59% is transformed into heat to be dissipated. From experimental testing data it is possible to know that losses are mainly radiated away by the plume and only some 40% is the heat directly transferred from the thruster to the structure;

4. Conditions for surfaces are always considered end of life conditions to simulate the worst condition; so it is assumed a total emissivity of 0.8 and a solar absorbance of 0.21<sup>20</sup>.

Under these assumptions, the thermal balance reads<sup>20</sup>:

$$\alpha_s SA \sin \theta + P = A_r \varepsilon \sigma T^4$$

where  $S$  is the solar flux,  $A$  the satellite area invested,  $\alpha_s$  the absorbance coefficient of surfaces, then  $P$  represents the power dissipated from the thrusters (+10% for margin). On the right side appear: the thermal radiator area ( $A_r$ ), the emissivity ( $\varepsilon$ ), Boltzmann constant ( $\sigma$ ) and the radiator absolute temperature ( $T$ ).

The radiating surface results to be of 0.76 m<sup>2</sup>. In the spacecraft configuration it is placed on the lateral surfaces, under the solar panels when satellite is closed. All equipment is maintained in the ranges required and the temperature during eclipse phases is about 282 K.

The Multi Layer Insulation (MLI) selected for the spacecraft external surface is MLI 10 due to its larger conductance and emissivity with respect to MLI 20. The MLI 20 insulation gives more protections from radiation, so it is recommended for the internal side of the spacecraft and to cover the critical components. The TCS mass breakdown is shown in Table 5-24.

	Size m <sup>2</sup>	Density [Kg/m <sup>2</sup> ]	mass [kg]
<b>MLI 20 layers</b>			
<b>internal</b>	1.68	0.6	1.0
<b>external</b>	0.45	0.6	0.27
<b>equipment</b>	0.2	0.6	0.12
<b>MLI 10 layers</b>			
<b>Solar Arrays</b>	1.26	0.36	0.45
<b>Radiator Surface</b>	0.76	0.78	0.59
<b>Total</b>			<b>2.44</b>

Table 5-24: Main thermal radiators and layers on spacecraft<sup>20</sup>.

### 5.17.1 Radiator surface specification

Each electrical component dissipates an amount of heat that is transferred by conduction and irradiation to the components around. This analysis is carried out considering the maximum dissipated power value when available in component datasheet; otherwise if no data are available an approximate value of 15% of the whole absorbed power has been assumed.

The following list presents the dissipated power values for the most critical components.

Components	Dissipated Power [W]
<b>Thruster</b>	94
<b>PCU</b>	25
<b>FEEP</b>	1
<b>Cold Gas</b>	1
<b>Data recorder</b>	2.25
<b>Primary computer</b>	1.5
<b>Reaction wheel</b>	1.2

Table 5-25: Dissipated power values for the most critical components. All the others electrical components are neglected because they dissipate less than 1 W.

Radiator and multilayer surfaces are chosen to insulate and protect the electrical devices and to passively convey the heat outside the satellite. Optical solar reflectors (OSR) are used to cover the three external radiating surfaces to disperse heating produced into deep space. In particular, OSR produced by JDSU are composed of vitreous material with Cerium oxide as an upper substrate covering a metal surface of silver as mirror plane.

The most relevant physical and thermo-optical characteristics of JDSU OSR are listed in Table 5-26.

<b>Thickness [<math>\mu\text{m}</math>]</b>	75-150
<b>Density [<math>\text{g}/\text{cm}^3</math>]</b>	2.5
<b>Solar Absorption Coefficient (<math>\alpha_s</math>)</b>	0.070
<b>Thermal Emission Coefficient (<math>\epsilon</math>)</b>	0.88

Table 5-26: Physical and thermo-optical properties of JDSU Optical Solar Reflectors (OSR)

Kapton and mylar multilayer are used to limit the heat flux between internal components. They are composed by a mylar film with deposited aluminium enclosed within a kapton film.

This particular layer configuration enables to passively insulate spacecraft components. A passive method to carry out the heating from the hot components such as thrusters it can represent by filler surfaces, thermal doublers and straps or braid. These elements can increase the heat conduction to other surfaces and to the external louvers. Doublers and straps materials could be aluminium alloys or Copper alloys wrapped in MLI surfaces to increase heat conduction, while interface fillers are usually formed as laminated graphite sheet or silicone elastomer, filled with boron nitride fibre.

Electrical heaters are also used to keep a component temperature within a specific range and to control the thermal gradient. In particular, Xenon tank must operate at temperature range between - +7 and +50 °C, while Butane tank operates between -20 and +60 °C. Accordingly, film heaters can be placed on the external side of the tank in order to keep each tank temperature at a suitable value. Next table summarize the power needed to tanks to conserve the right temperature:

	<b>Xenon Tank</b>	<b>Butane Tank</b>
<b>Satellite Temperature</b>	290 K	290 K
<b>Required Temp Tank</b>	300 K	300 K
<b>Area</b>	0,063 m <sup>2</sup>	0,044 m <sup>2</sup>
<b>Power Required</b>	3,67 W	2,56 W

Table 5-27: Required heat for Xenon and Butane tanks.



## 5.18 Spacecraft Communication Subsystem

The spacecraft communication subsystem will consist of the following functional units (modules).

- Antenna system
- Antenna switch matrix
- Transmitter signal generation module
- Transmitter RF power amplifier module
- Receiver RF front end module
- Receiver signal processing module
- Reference frequency generation module
- Control module

The communication subsystem should be able to provide required telecommand and telemetry and satellite ranging support capabilities.

The communication subsystem will be designed to operate in S-band frequency range (2.1 - 2.3 GHz) using BPSK modulation at typical data rate of 50 kbits/s.

The actual transmit power and data rate should be adjustable over relatively wide range due to varying radio link conditions caused by highly elliptical orbit of the spacecraft.

Table 5-28 shows the preliminary mass budget of the Spacecraft Communication Subsystem (SCS).

	n°	Mass [kg]
<b>Helix antennas</b>	1	0.11
<b>Patch Antenna</b>	2	0.16
<b>Cabling</b>	1	0.13
<b>Antenna Switch Matrix</b>	1	0.15
<b>Transmitter Signal Generation Module</b>	1	0.2
<b>Transmitter RF Power Amplifier</b>	1	0.8
<b>Receiver RF Front-end Module</b>	1	0.3
<b>Receiver Signal Processing Module</b>	1	0.2
<b>Reference Frequency Generation</b>	1	0.1
<b>Control Module</b>	1	0.1
<b>Additional Cabling Mass</b>	1	0.08
<b>Total</b>		<b>2.33</b>

Table 5-28: Spacecraft Communication Subsystem mass breakdown.

## 5.18.1 Antenna System

Two different commercial antennas operating in the S band are chosen. In particular, two SSTL micro patch low frequency S-Band omni-directional antennas<sup>22</sup> and one medium gain AntDevCo helix antenna<sup>23</sup> capable of supporting very high data rates up to 25 W of transmitted power are considered. Most relevant specifications of patch and helix antennas are listed in Table 5-29 and 4-29, respectively.

<b>SSTL Micropatch Low Frequency S-Band Omni-directional Antenna</b>	
<b>Gain [dB]</b>	3
<b>Frequency [MHz]</b>	2000 – 2500
<b>Dimensions [mm]</b>	82 x 82 x 20
<b>Mass [g]</b>	80
<b>Op. Temperature [°C]</b>	-20 to 50
<b>Power [W]</b>	<10
<b>Heritage:</b> RapidEye, Deimos-1, NigeriaSat-2	




Table 5-29 SSTL Micropatch antenna specifications.

<b>AntDevCo Helix Antenna</b>	
<b>Gain [dB]</b>	9
<b>Frequency</b>	2000 - 2300
<b>Bandwidth [MHz]</b>	300
<b>Dimensions [mm]</b>	φ100 x 150
<b>Mass [g]</b>	110
<b>Temperature [°C]</b>	-150 to 95
<b>Power [W]</b>	<25
<b>Heritage</b> NASA Genesis mission	




Table 5-30: AntDevCo helix antenna specifications.

## 5.18.2 Antenna Switch Matrix

The antenna switch matrix should provide selection of the antenna with highest gain towards the groundstation for both transmitter and receiver. Information from the spacecraft attitude determination system can be used when making decisions which antenna to select. It should also provide necessary switching and sequencing functionality to switch between transmit and receive modes and protection of the spacecraft receiver input from the transmitter RF output signal



# E-sail Demo Preliminary Design

Doc. No.: -  
Issue: 1.0  
Date: Nov. 20, 2011  
Page: 59 of 72

leakage. It can be implemented by using solid state PIN diode devices or electromechanical switches and it should be enclosed with RF shielded enclosure.

The estimated peak power consumption during switching is 300 mW, if electromechanical switches are used, or 200 mW if PIN diode switches are used.

### 5.18.3 Transmitter Signal Processing Module

The transmitter signal processing module should be able to generate low level BPSK modulated RF signal with requested data rate and error correction scheme providing necessary shaping and filtering of the modulated RF signal. It should also be able to generate ESA satellite ranging system compatible ranging signals.

The transmitter signal processing module can be implemented based on FPGA or dedicated RF circuits or combination of both. Should be enclosed in RF and eventually radiation shielded enclosure. The estimated peak power consumption is 300mW in transmit mode while only 1mW is required in standby.

### 5.18.4 Transmitter RF Power Amplifier

The transmitter RF power amplifier should be able to amplify the low level modulated RF signal to the specified level (10W) with good efficiency (>40%) providing also necessary additional filtering to suppress unwanted harmonics and spurious emissions of the RF signal. Moreover, it provides the functionality to be able to adjust the output power between 100 mW and 20 W by approximately 1dB steps and the necessary thermal interface to be able to radiate dissipated power (max 10-15W).

It can be implemented using GAsFET or LDMOS transistors to achieve necessary gain and output power and it should be enclosed in RF and eventually radiation shielded enclosure with adequate thermal interface. The estimated peak power consumption is 50W at full output power and 100% duty cycle and 1mW in standby mode.

### 5.18.5 Receiver Front-end Module

The receiver front-end module should provide necessary RF filtering and amplification of the incoming RF signal and it should have low enough noise figure and acceptable dynamic range.

It can be implemented by using low noise PHEMT transistors and ceramic cavity filters for RF filtering. The receiver front-end module needs RF and radiation shielding. Its estimated peak power consumption is 300 mW.



## **E-sail Demo Preliminary Design**

Doc. No.: -  
Issue: 1.0  
Date: Nov. 20, 2011  
Page: 60 of 72

### **5.18.6 Receiver Signal Processing Module**

The receiver signal processing module should be able to amplify, filter and demodulate the telecommand RF signal from the RF front end module and to amplify, filter and demodulate the RF signal used for satellite ranging purposes and extract the necessary timing information.

It can be implemented based on FPGA or dedicated RF circuits or combination of both. It is possible to use a Software Designed Radio (SDR) type architecture. It should be enclosed in RF and eventually radiation. Its estimated peak power consumption is 200 mW.

### **5.18.7 Reference Frequency Generation Module**

The reference frequency generation module should provide necessary high accuracy ( $<0.01\text{ppm}$ ) and stable reference frequency for the transmitter, receiver and other spacecraft subsystems if necessary. Reference frequency generation unit can be implemented as an oven controlled crystal oscillator (OCXO) considering many space qualified alternatives available from different manufacturers with an estimated power consumption smaller than 3W (mostly heating power depending on the actual temperature environment).

### **5.18.8 Stored Data Preliminary Estimation**

The amount of data stored on board that have to be transmitted to the ground station has been preliminary estimated to perform the downlink communication link budget. In order to obtain a conservative assessment of the quantity of data that have to be stored and transmitted, the period of final orbit has been assumed as reference value and a total of 66 channels, including the sensors required both for spacecraft and payload operations, have been considered. In particular, 12 temperature sensors have been assumed for the spacecraft and 12 for the Hall and FEED thrusters. Moreover, 18 temperature sensors are required for the 3 deployed solar arrays, the batteries, the tanks and the electronics. A total of 14 sensors are required to monitor spacecraft attitude and the payload. Table 5-31 shows the total amount of stored data over one orbit.

Sensor	Chann.	Frequency[Hz]	Precision [bit]	Stored Data[Mbit]
<b>FEEP Temp. Sensors</b>	4	0,1	16	1,62
<b>HET Temp. Sensors</b>	8	0,1	16	3,24
<b>SC Internal Temp. Sensors</b>	12	0,1	16	4,85
<b>SA Temp. Sensors</b>	6	0,1	16	2,43
<b>Batteries Temp. Sensors</b>	2	0,1	16	0,81
<b>Tanks Temp. Sensors</b>	4	0,1	16	1,62
<b>Electronics Temp. Sensor</b>	6	0,1	16	2,43
<b>Sun Sensor</b>	4	0,1	16	1,62
<b>Earth Sensor</b>	1	0,1	16	0,40
<b>Magnetometer</b>	4	0,1	16	1,62
<b>Accelerometer</b>	4	0,1	16	1,62
<b>Electron Spectrometer</b>	1	0,1	16	0,40
<b>Others</b>	10	0,1	16	4,04
<b>Total</b>	<b>66</b>			<b>26,69</b>

Table 5-31: Total amount of stored data from spacecraft sensors over one orbit.

Considering storing the data once every 10 seconds over the whole orbit, a total of 26.7 Mb have to be stored in the data recorder and downloaded to the ground station during communication phases.

### 5.18.9 Link Budget

Many alternative possibilities exist for the ground stations. In order to give a preliminary estimate of the expected link performance, two ground stations controlled by the Italian Space Agency (ASI) have been considered as candidates for the E-sail Demo mission (Table 5-32).

Station	Latitude (deg, N)	Longitude (deg, E)	Altitude (m)	Position
<b>MAT</b>	40.65	16.704	543	Matera; Italy
<b>MAL</b>	-2.996	40.195	12	Malindi; Kenya

Table 5-32: Position of the candidate ground stations.

Considering the ground track of the spacecraft during the whole mission (see Figure 24), the ground station visibility for the two candidate stations can be assessed.

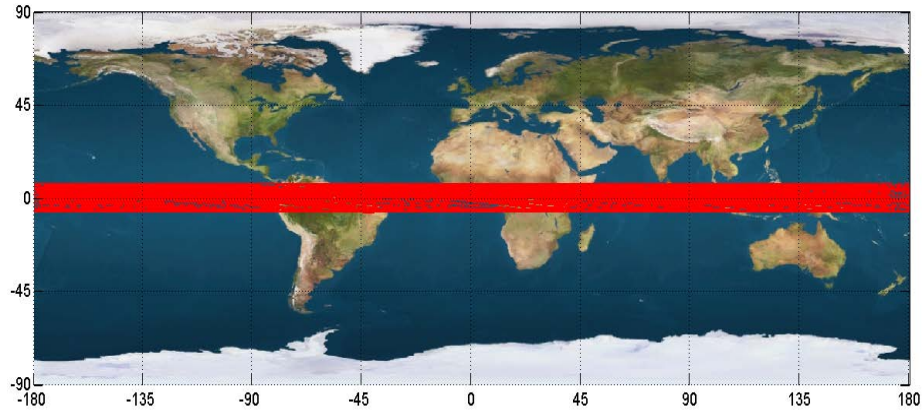


Figure 24: Spacecraft Groundtrack.

Figure 25 shows the ground stations visibility of the Matera ground station (left) and the Malindi ground station (right) during the whole mission lifetime.

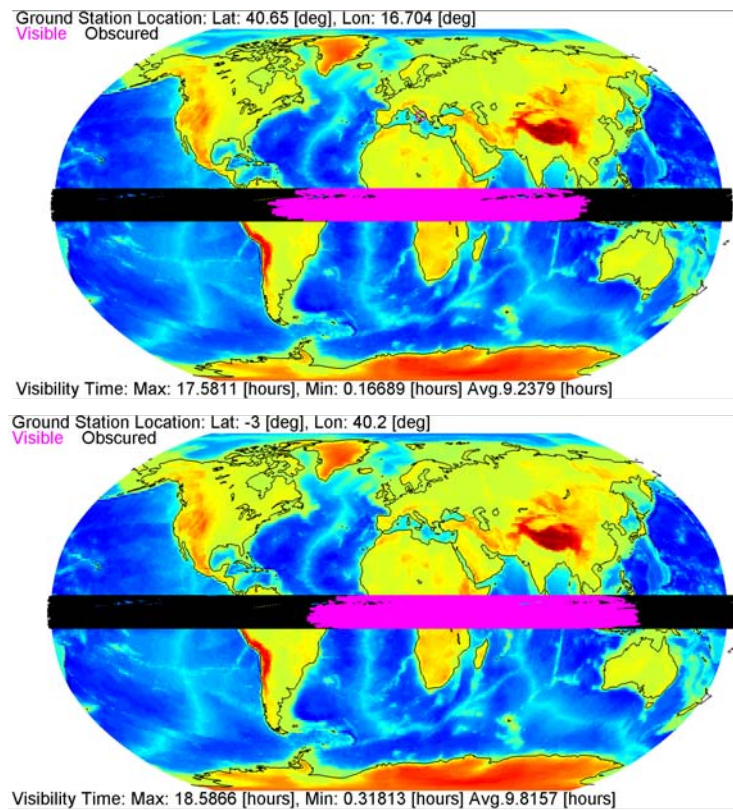


Figure 25: Ground station visibility for the Matera ground station (left) and the Malindi ground station (right).



## E-sail Demo Preliminary Design

Doc. No.: -  
Issue: 1.0  
Date: Nov. 20, 2011  
Page: 63 of 72

Considering the average visibility time of the two ground stations, the Malindi station has been selected for further analyses. The Malindi station provides tracking capabilities in S-band (transmit and receive) and L- and X-band (receive). The station hosts a 10 m<sup>2</sup> antenna with an elevation -12.75 metres and is equipped with a no-break power plant.

Considering the available communication band, the medium gain antenna (Helix) is assumed to be used for data downlink and the micropatch S-band antenna for data uplink. The communication margin has been assessed considering the characteristics of antennas described in Sec. 5.18.1.

Some conservative preliminary assumptions for the link budget have been considered:

1. A minimum transmission data rate of 50 kbps;
2. Maximum spacecraft altitude during communication phase of 20000 km;
3. A communication bit error rate (BER) of 10e-5, using a Binary Phase Shift Keying (BPSK) modulation technique;
4. Implementation equal to 2 dB.

Table 5-33 shows the link budget.

The resulting margin for the spacecraft preliminary link budget with the Malindi ground station is equal to 12.8 dB. Considering 2 dB for rain degradation this value is further reduced to 10.8 dB.

Considering the maximum amount of data stored in the data recorder (26.69 Mb), less than 10 minutes of data downlink are sufficient to transfer all the data to the ground station.

The present analysis, carried out considering Malindi ground station, only represents a reference situation and similar or slightly reduce performance (in terms of link budget margin and data transmission time) could be obtained considering a network of radio amateur ground stations.

Item		Unit	Value
Frequency	f	GHz	2.30
Transmitter power	P	W	10.00
Transmitter power	P	dBW	10.00
Trasmitter Line Loss	$L_i$	dB	-1.00
Transmit Antenna Beamwidth	$\theta_t$	deg	72.00
Peak Transmit Antenna Gain	$G_{pt}$	dBi	9.00
Transmit Antenna Diameter	$D_t$	m	0.10
Transmit Antenna Pointing Offset	$e_t$	deg	65.70
Transmit Antenna Pointing Loss	$L_{pt}$	dB	-10.00
Transmit Antenna Gain (net)	$G_t$	dBi	-1.00
Equiv. Isotropic Radiated Power	EIRP	dBW	8.00
Space Loss	$L_s$	dB	-185.70
Atmospheric Loss	$L_a$	dB	-0.23
Receive Antenna Diameter	$D_r$	m	10.00
Peak Receive Antenna Gain (net)	$G_{rp}$	dB	46.50
Receive Antenna Beamwidth	$\theta_r$	deg	1.00
Receive Antenna Pointing Error	$e_r$	deg	0.50
Receive Antenna Pointing Loss	$L_{pr}$	dB	-3.00
Receive Antenna Gain	$G_r$	dB	43.50
System Noise Temperature	$T_s$	K	64.00
Data Rate	R	bps	50000
$E_c/N_0$ (1)	$E/N_0$	dB	26.10
Carrier-to-Noise Density Ratio	C/N <sub>0</sub>	dB-Hz	73.10
Bit Error Rate	BER	-	1.0e-7
Required $E_b/N_0$ (2)	$(E/N_0)_r$	dB	11.30
Implementation Loss (3)	-	dB	-2.00
Margin	-	dB	12.80

Table 5-33: Spacecraft preliminary link budget with Malindi ground station.



## 5.19 Spacecraft Structure

Considering the total available ASAP 5 fairing volume, the spacecraft structure preliminary design has been carried out aiming at obtaining the maximum possible area for the solar arrays and internal volume for all the spacecraft subsystems. Thus, the structure appears as a box with 2 internal bays and three deployable solar panels. The lower bay is dedicated to thrusters and feeding system and the upper one, representing the larger volume, accommodates all the other spacecraft equipment (tanks, batteries, reaction wheels, electronics, etc. etc.).

The ASAP interface flange is positioned on the top of the spacecraft together with some Earth and Sun sensors, the medium gain antenna and some components of the payload. On the bottom side of the spacecraft the two Alta HT-400 Hall Effect Thrusters are placed within a 400x180 mm<sup>2</sup> cavity to avoid direct plasma sputtering on the other components. The main spacecraft frame structural elements are represented by four standard commercial C-shaped columns. The materials adopted for the structure are 7075 and 6061 aluminum alloys. Table 5-34 lists the most relevant physical characteristics and mechanical properties of the materials used.

	Density (kg/m <sup>3</sup> )	Young's modulus E (GPa)	Yield strength Sy (MPa)
<b>6061 T6</b>	2800,00	68,00	276,00
<b>7075 T6</b>	2700,00	71,00	503,00

Table 5-34: Physical characteristics of the aluminium alloys composing the spacecraft structure.

Table 5-35 shows the mass of spacecraft structure elements.

	Structure		
	Mass [kg]	Q.ty	Tot [kg]
<b>Base plate</b>	1,5	1	1,5
<b>Internal Plate</b>	1,1	2	2,2
<b>Side plate</b>	0,43	4	1,72
<b>Column</b>	0,33	4	1,32
<b>Total Mass</b>			6,74

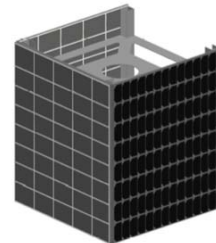


Table 5-35: Elements of spacecraft structure and their mass.

## 5.19.1 Solar Panels Structure

The structure of the three deployable solar panels is composed by space-proven sandwich composite materials with a honeycomb core of aluminum for a total thickness of 10 mm. Panels are attached to the front side of the spacecraft by means of two joints per panels. Joints are composed by two plate assembled on the internal surface of the panel and then assembled with the structure. A pre-loaded helical spring enables the panel deployment.

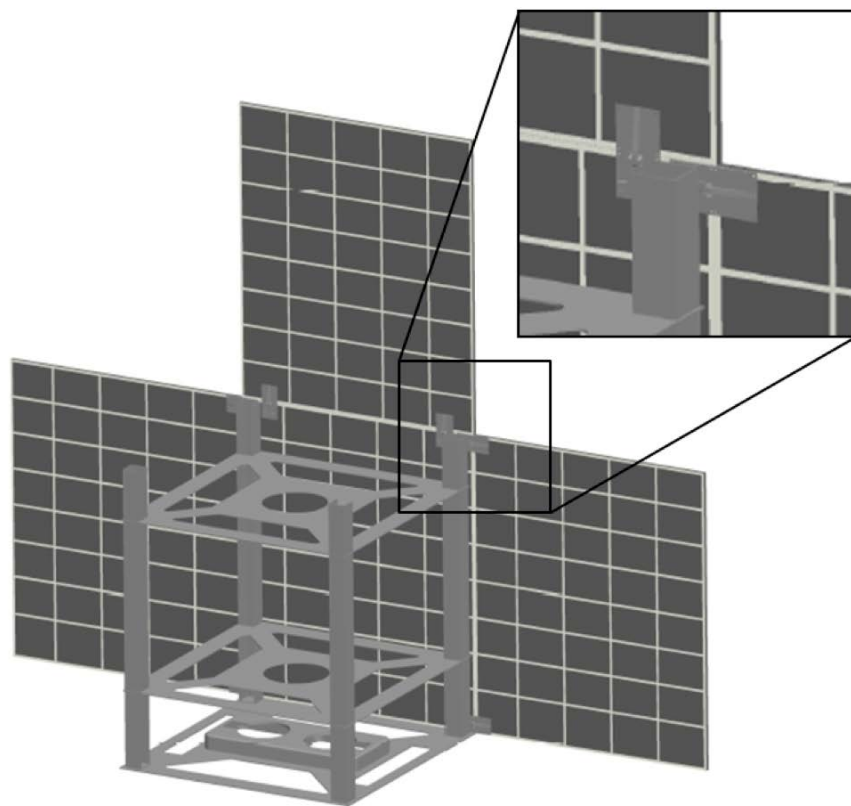


Figure 26: Spacecraft structure and detail of solar panels deployment joint.

## 6 POWER BUDGET

The total power required by the most relevant spacecraft subsystems during the mission is about 420 W (see Table 6-1).

Subsystem	Power [W]
<b>SPS</b>	375
<b>AOCS</b>	20
<b>Thermal</b>	10
<b>PGS</b>	15
<b>SCS</b>	50
<b>C&amp;DH</b>	2
<b>Payload</b>	70

Table 6-1: Power required by the most relevant spacecraft subsystems during the mission.

Considering the relevant amount of power required by the thruster, it is assumed to avoid thruster operations during eclipse phases. The required power is shown in Table 6-2.

Subsystem	Orbit Transfer Mode	Eclipse Mode	Data Transmission Mode	Payload Operation Mode
<b>SPS</b>	375 W	0 W	0 W	0 W
<b>AOCS</b>	20 W	20 W	20 W	20 W
<b>Thermal</b>	10 W	10 W	10 W	10 W
<b>PGS</b>	15 W	15 W	15 W	15 W
<b>SCS</b>	0 W	0 W	50 W	0 W
<b>C&amp;DH</b>	2 W	2 W	2 W	2 W
<b>Payload</b>	0 W	0 W	0 W	30 W
<b>Total</b>	<b>422 W</b>	<b>47 W</b>	<b>97 W</b>	<b>77 W</b>
<b>Incoming Power</b>	<b>478 W</b>	<b>478 W</b>	<b>478 W</b>	<b>478 W</b>
<b>Margin</b>	<b>56 W</b>	<b>431 W</b>	<b>381 W</b>	<b>401 W</b>

Table 6-2: Power required by the spacecraft and by each subsystem during the most relevant phases of the mission.

The maximum power required by the spacecraft, during the orbit transfer mode, is 430 W while the maximum power that can be generated is about 470 W. Thus, at spacecraft beginning of life, slightly more than 50 W of power are available for battery charging if required. Considering a conservative value for solar panels degradation of 10%, at the spacecraft end of life the maximum generated power is about 430 W.

## APPENDIX A

Outline drawings of the spacecraft.

